Magnetic helicity in astrophysical dynamos

Simon Candelaresi

Cover image: Volume rendering of the magnetic energy for the 9-foil knot.

ISBN 978-91-7447-593-7

Printed in Sweden by Universitetsservice, US-AB, Stockholm 2012
Distributor: Department of Astronomy, Stockholm University

Abstract

The broad variety of ways in which magnetic helicity affects astrophysical systems, in particular dynamos, is discussed.

The so-called α effect is responsible for the growth of large-scale magnetic fields. The conservation of magnetic helicity, however, quenches the α effect, in particular for high magnetic Reynolds numbers. Predictions from mean-field theories state particular power law behavior of the saturation strength of the mean fields, which we confirm in direct numerical simulations. The loss of magnetic helicity in the form of fluxes can alleviate the quenching effect, which means that large-scale dynamo action is regained. Physically speaking, galactic winds or coronal mass ejections can have fundamental effects on the amplification of galactic and solar magnetic fields.

The gauge dependence of magnetic helicity is shown to play no effect in the steady state where the fluxes are represented in form of gauge-independent quantities. This we demonstrate in the Weyl-, resistive- and pseudo Lorentz-gauge. Magnetic helicity transport, however, is strongly affected by the gauge choice. For instance the advecto-resistive gauge is more efficient in transporting magnetic helicity into small scales, which results in a distinct spectrum compared to the resistive gauge.

The topological interpretation of helicity as linking of field lines is tested with respect to the realizability condition, which imposes a lower bound for the spectral magnetic energy in presence of magnetic helicity. It turns out that the actual linking does not affect the relaxation process, unlike the magnetic helicity content. Since magnetic helicity is not the only topological variable, I conduct a search for possible others, in particular for non-helical structures. From this search I conclude that helicity is most of the time the dominant restriction in field line relaxation. Nevertheless, not all numerical relaxation experiments can be described by the conservation of magnetic helicity alone, which allows for speculations about possible higher order topological invariants.

Acknowledgments

The content of this work has been a collaborative effort with the co-authors on the publications. Their input has been fundamental for the progress of this entire work. Through discussions my overall understanding of the matter presented here has benefited considerably.

Of course I thank my supervisor **Axel Brandenburg**, not only for the supervision, but especially for the encouragements for pursuing my own projects and start collaborations with scientists, even outside this narrowly defined field.

I appreciate the efforts by **Dhrubaditya Mitra** and **Matthias Rheinhardt** for clearly explaining the complex matter we are working with and helping with the PENCIL CODE, which often works in mysterious ways.

Getting into the world outside my working group has been possible with the help of **Anthony Yeates** and **Nobumitsu Yokoi** who hosted me at their home institutes and with whom we had discussions during my stay. Although the collaborative work has not made it into this thesis it has greatly broadened my perspectives and will surely lead to conclusive work in the near future.

With **Chi-Kwan Chan**, **Alexander Hubbard** and **Gustavo Guerrero** we had various helpful discussions about physics, numerics, computing and the PENCIL CODE, which helped in progressing this work. Without fellow PhD students **Fabio Del Sordo**, **Jörn Warnecke** and **Koen Kemel**, as well as **Alessandra Cagnazzo** and **Elizabeth Yang** the entire time would have been rather dull. So thanks goes for keeping me away from work and keeping me sane.

Of course thanks goes to **Hans von Zur-Mühlen** for helping with various technical issues and proof reading the Swedish summary of this thesis and **Fabio Del Sordo** for corrections in the thesis.

Special appreciation goes to **Carola Eugster** for her tireless encouragements throughout the whole project and for patiently improve various important texts written during my time as grad student.

Without the professional tools developed by the **open source community** all the research related work would have progressed in a much slower pace. Naming all the contributors would require several phone books, so just a few should be mentioned here: **Linus Torvalds** for developing Linux, **Donald Knuth** and **Leslie Lamport** for developing TEX and LATEX, **Axel Brandenburg** and **Wolfgang Dobler** for the PENCIL CODE, **Guido van Rossum** for Python and **John Hunter** for matplotlib.

Even for-profit ventures should be thanked for making this work possible, in particular the **Asus company** for coming up with highly mobile electronics which can be used to do actual work. Without it I couldn't have met all the deadlines while constantly traveling.

Most of the sacrifices for this work were endured by two reliable workhorses who almost never complained: **HP Pavilion Entertainment** and **Asus Eee PC 1015BX**.

Further work horses have been the computers at the **Center for Parallel Computers at the Royal Institute of Technology** in Sweden and Iceland, the **National Supercomputer Centers in Linköping**, the **QMUL HMC facilities** and the **Carnegie Mellon University Supercomputer Center**.

This work has been supported in part by the **European Research Council** under the AstroDyn Research Project 227952 and the **Swedish Research Council** grant 621-2007-4064.

List of Papers

The following papers are included in this thesis. They are referred to in the text by their Roman numerals,

I **Candelaresi, S.** and Brandenburg, A.: 2012, "The kinetic helicity needed to drive large-scale dynamos", *Phys. Rev. E*, submitted, arXiv: 1208.4529

II Brandenburg, A., **Candelaresi, S.** and Chatterjee, P.: 2009, "Small-scale magnetic helicity losses from a mean-field dynamo", *Mon. Not. Roy. Astron. Soc.*, **398**, 1414

III Mitra, D., **Candelaresi, S.**, Chatterjee, P., Tavakol, R. and Brandenburg, A.: 2010, "Equatorial magnetic helicity flux in simulations with different gauges", *Astron. Nachr.*, **331**, 130

IV **Candelaresi, S.**, Hubbard, A., Brandenburg, A. and Mitra, D.: 2011, "Magnetic helicity transport in the advective gauge family", *Phys. Plasmas*, **18**, 012903

V Del Sordo, F., **Candelaresi, S.** and Brandenburg, A.: 2010, "Magnetic-field decay of three interlocked flux rings with zero linking number", *Phys. Rev. E*, **81**, 036401

VI **Candelaresi, S.** and Brandenburg, A.: 2011, "Decay of helical and non-helical magnetic knots", *Phys. Rev. E*, **81**, 016406

My contribution to the papers

I For this work I did most of the simulations and evaluations. I also wrote most of the text.

II I performed a few simulations and contributed in writing and editing the text.

III My contributions for this work were analyzing the results and editing the text.

IV I performed all the simulations and did most of the evaluations. I was also responsible for the text which was mostly written by myself.

V The idea for this work came out of a course on solar physics. I performed some of the simulations and contributed to the evaluation. Writing the text was done jointly with the co-authors.

VI This project came out of my initiative and was completely conducted by myself. I did the simulations for which I modified and extended the used numerical code. The evaluations were done by me as well as writing the text.

Contents

1. Introduction

Je n'ai fait celle-ci plus longue
que parce que je n'ai pas eu le loisir
de la faire plus courte.

I would have written a shorter letter,
but I did not have the time.

Blaise Pascal

Asking astronomers about the relevant forces for the dynamics of astrophysical objects the only answer is often "gravity". Gravity is undoubtedly responsible for the structures we see at scales of the Universe. But what is often forgotten is the effect of electromagnetic forces, which often goes beyond radiation pressure. For accretion discs magnetic fields lead to angular momentum transport and ensure quick spin-downs. The presence of magnetic fields in planets and stars provides shielding from charged and energetic particles and suppresses convection. Starspots and sunspots, which are highly magnetized regions, are ares of reduced radiation.

Observations of magnetic fields in the universe date as far back as 364 BCE, when Chinese astronomers observed sunspots for the first time. Of course back then little was known about their magnetic nature. It was thanks to Galileo Galilei that sunspots were recorded more systematically, which has been continued ever since and created an almost complete record spanning four centuries. Their occurrence was explained in 1908 by George Ellery Hale who first obtained Zeeman measurements from the Sun's surface, which revealed strong magnetic fields of ca. 2 kG on sunspots. This strong field suppresses convective motions that would otherwise replenish the surface with hot material. The temperature in those regions drops due to thermal radiation which makes them appear dark. Typical life times are between days and up to 3 months during which proper motion can be observed.

The occurrence of sunspots is not random in time, nor are they randomly distributed on the Sun's surface. Within 11 years the total number observed varies between maximum and minimum during which almost no spots are observed (Fig. 1.1, lower panel). We can trace this behavior back to the first systematic observations in 1610. The only period during which this striking rule does not apply is the so-called Maunder minimum from ca. 1650 to 1700, during which almost no sunspots were observed. At the beginning of each cycle the first sunspots appear at latitudes of around 30 degrees. As time evolves

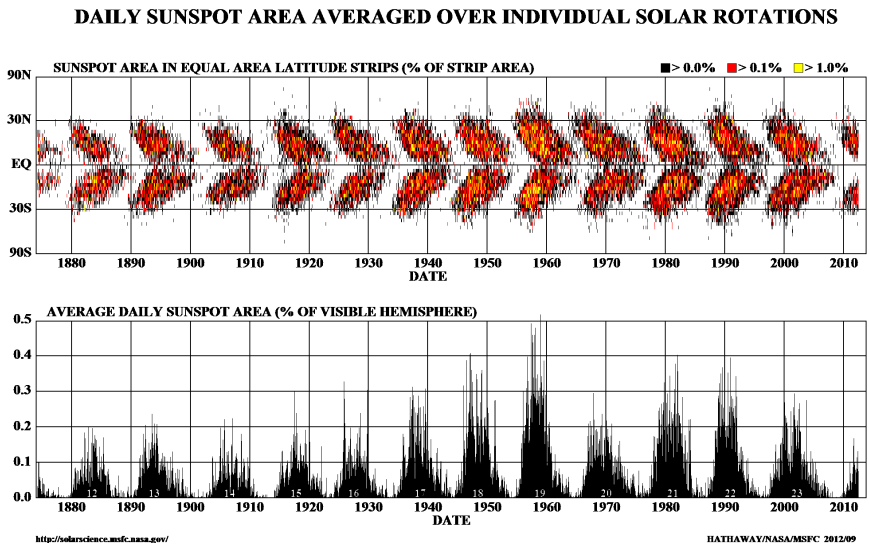

Figure 1.1: Longitudinally averaged area covered by sunspots (upper panel). Percentage of the visible hemisphere covered with sunspots (lower panel). (NASA 2012)

they emerge closer to the equator. Plotting the longitudinal average of the area covered with sunspots gives a butterfly-like diagram (Fig. 1.1, upper panel). Today we can measure all three spatial components of the Sun's magnetic field. One of the most striking revelations from these magnetograms is the reversal of the sign of the magnetic field after every 11 years. This 22 years periodic cycle is the magnetic cycle (Fig. 1.2).

Explaining the occurrence of the Sun's magnetic field first led to the primordial theory, which claims that the creation of the field happened during the Sun's formation from an interstellar gas cloud. Since the hot gas is highly conducting it is plausible that via an induction mechanism potential energy can be partially transformed into magnetic energy. Of course one would need to take into account the full energy balance, which further includes kinetic and thermal energy. Both the large scale and the strength of the field can be explained by this theory. But it falls short in clarifying the cyclic behavior and how it could have outlived 4.5 billions of years of resistive decay.

To address those drawbacks, a mechanism is necessary that constantly regenerates magnetic fields on scales which we observe on the Sun. At the same time it has to explain how the cyclic behavior comes about. The most successful and generally accepted theory is the dynamo theory, which explains how turbulent motions in a conducting medium give rise to magnetic fields of ener-

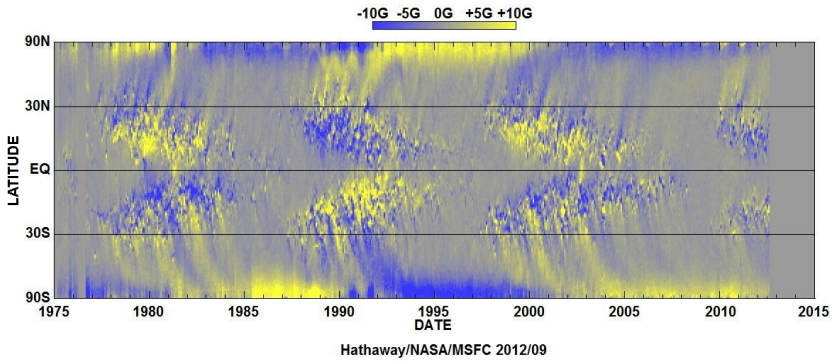

Figure 1.2: Polar magnetic field strength at various latitudes for the Sun. The magnetic active regions coincide with the sunspots. This diagram is often referred to as the magnetic butterfly diagram. (NASA 2012)

gies comparable to the energies of the motions and scales similar to the system size. Turbulent dynamos provide a convincing mechanism for the Sun's magnetic field. Other than the Sun also galactic fields and fields of accretion discs can be explained by this mechanism (Brandenburg et al., 1995).

An important ingredient of turbulent dynamos is kinetic helicity of the turbulent motions, i.e. the scalar product of the velocity with the vorticity. As a result the magnetic field will be helical as well, with helicities of opposite signs in the small and large scales. The presence of small-scale magnetic helicity, however, reduces the production of large-scale magnetic energy, which is produced by small-scale helical motions. For a closed system this means that the field reaches saturation only on time scales determined by the resistivity, which are much longer than the relevant dynamical time scales for astrophysical systems. A quantitative study of the dynamo's behavior for a closed system is presented in **Paper I**, where we investigate conditions under which dynamo action occurs and how the saturation state depends on relevant parameters. This work was motivated by recent findings about the onset of large-scale dynamo action of Pietarila Graham et al. (2012) that did not agree with standard models of Blackman and Brandenburg (2002), confirmed in Käpylä and Brandenburg (2009).

Open systems can reduce the amount of magnetic helicity via fluxes. This reduces the dynamo quenching coming from the presence of small-scale magnetic helicity significantly (**Paper II**). In practical terms it means that astrophysical dynamos must have some mechanism by which helicity is shed. For the Sun one candidate is coronal mass ejections, which frequently occur where

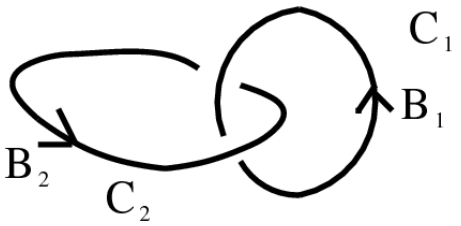

Figure 1.3: Mutually linked magnetic fluxed tube make up one of the simplest helical field configurations.

the field is strongly twisted, i.e. helical.

Magnetic helicity density is the scalar product of the magnetic vector potential $\boldsymbol{A}$ and the magnetic field $\boldsymbol{B}$. Potentials are always defined up to a gauge, which can be chosen freely. That means that magnetic helicity density and its fluxes are dependent on the gauge choice. The conditions under which a dynamo is excited must, however, not depend on the gauge. In **Paper III** and **Paper IV** both magnetic helicity fluxes and transport are investigated. Luckily for the dynamo, the physically relevant quantities, like the time averaged fluxes in the statistically steady state, turn out to be gauge-independent.

To illustrate magnetic helicity, one can think of magnetic flux tubes, which are twisted like a helix, with both ends connected. Helices are not the only helical fields one can think of. Two flux tubes, which are mutually linked, constitute a helical configuration as well (Fig. 1.3). Letting such fields evolve leads to a reduction of magnetic energy through various channels. Resistivity slowly destroys magnetic energy, while reconnection, i.e. braking and connecting magnetic field lines, has a faster effect. Reconnection is, however, a violent process and hence not favored in field relaxation. If we cannot rely on reconnection being effective enough, a helical system of the kind of interlocked flux rings cannot freely evolve due to the conservation of mutual linkage. This restriction is captured in the *realizability condition*, which gives a lower bound for the magnetic energy in presence of magnetic helicity. Unfortunately the overly simple picture of linked field lines can be broken by an idealized non-helical configuration composed of linked field lines. What happens then is part of **Paper V**, where the relaxation of linked, helical and non-helical fields is investigated.

Magnetic helicity is not the only quantity, which quantifies the field's topological structure. There exists an infinite number of topological invariants. Whether or not such invariants could give restrictions on the relaxation is studied in **Paper VI**, in which helical and non-helical knots and links are investigated.

The approach taken in this work is purely theoretical. No observations have been consulted to make quantitative comparisons with the results. Yet, observations provided the impulse for all the investigations. All the setups are investigated within the framework of magnetohydrodynamics, which provides a reasonable description of the physical systems. Solving these non-linear partial differential equations is done numerically using the PENCIL CODE[1], a high-order finite difference PDE solver.

[1] http://pencil-code.googlecode.com

2. Framework

O studianti, studiate le matematiche,
e non edificate sanza fondamenti.

Therefore O students study mathematics
and do not build without foundations.

Leonardo da Vinci

2.1 Magnetohydrodynamics

Through observations of turbulent motions we know that astrophysical plasma are viscous media. The dynamics of viscous flows is described via the Navier-Stokes equations, which couple the velocity field with the density, the pressure and the viscous forces. Charge separation makes the media highly conducting, which brings the Maxwell equations into play which couple the charges and currents with the electromagnetic field. Combining the Navier-Stokes and Maxwell equations gives the equations of magnetohydrodynamics (MHD) for conducting fluids. The coupling between the velocity and electromagnetic field comes from the Lorentz force.

Differing inertia of electrons and positive ions make plasma sophisticated media to study, in particular in relativistic environments. For those systems studied here the inertia of the charge carrying particles can be neglected. As a consequence any charge separation will be balanced within fractions of the here relevant time scales, which leaves the medium charge neutral. In addition the conductivity of the medium is high enough such that the electric field can be neglected. Further, the maximum velocities of such media are often much less than the speed of light. Hence, the displacement current can be neglected in favor of the electric current density $\boldsymbol{J}$ from Ohm's law.

Under these realistic simplifications the MHD equations for an isothermal medium read:

$$\frac{\partial \boldsymbol{A}}{\partial t} = \boldsymbol{U} \times \boldsymbol{B} - \eta \mu_0 \boldsymbol{J}, \tag{2.1}$$

$$\frac{\mathrm{D}\boldsymbol{U}}{\mathrm{D}t} = -c_\mathrm{s}^2 \boldsymbol{\nabla} \ln \rho + \boldsymbol{J} \times \boldsymbol{B}/\rho + \boldsymbol{F}_\mathrm{visc} + \boldsymbol{f}, \tag{2.2}$$

$$\frac{\mathrm{D} \ln \rho}{\mathrm{D}t} = -\boldsymbol{\nabla} \cdot \boldsymbol{U}, \tag{2.3}$$

with the magnetic vector potential $\boldsymbol{A}$, the velocity $\boldsymbol{U}$, the magnetic field[1] $\boldsymbol{B} = \boldsymbol{\nabla} \times \boldsymbol{A}$, the magnetic diffusivity η, the isothermal speed of sound c_s, the fluid density ρ, the electric current density $\boldsymbol{J} = \boldsymbol{\nabla} \times \boldsymbol{B}/\mu_0$, the external forcing $\boldsymbol{f}$ and the advective time derivative $\frac{\mathrm{D}}{\mathrm{D}t} = \frac{\partial}{\partial t} + \boldsymbol{U} \cdot \boldsymbol{\nabla}$. In the following discussions I will use units for which $\mu_0 = 1$. The viscous force is given by

$$\boldsymbol{F}_\mathrm{visc} = \rho^{-1} \boldsymbol{\nabla} \cdot 2\nu\rho\mathsf{S}, \tag{2.4}$$

with the traceless rate of strain tensor

$$\mathsf{S}_{ij} = \frac{1}{2}\left(U_{i,j} + U_{j,i}\right) - \frac{1}{3}\delta_{ij}\boldsymbol{\nabla} \cdot \boldsymbol{U} \tag{2.5}$$

for a viscous monatomic gas with the viscosity ν. For all the systems in this work isothermality is assumed where the pressure is given as $p = \rho c_\mathrm{s}^2$. Anything else would change the equation of state and lead to an additional equation which involves internal energies in the form of temperature.

2.2 Amplification of Magnetic Fields

Typical strengths of magnetic fields observed in stars and galaxies are of the order of the equipartition value, i.e. their energies are comparable with the kinetic energy of the turbulent motions and scales comparable with the system size. A mechanism is needed to explain the efficient conversion between kinetic and magnetic energies such that the resulting magnetic field has sizes similar to the dimensions of the system. The large scales should be contrasted to the scales of the turbulent eddies. Similar to the electromagnetic dynamo, where mechanical work is transformed into electromagnetic energy, in astrophysical objects there exists a similar mechanism for transforming energies. The relevant induction equation for this case is equation (2.1).

The energy input for the turbulent motions can be easily explained to come from convection where heat provides a source for kinetic energy on large scales through the buoyant rise of material. In a nearly inviscid fluid large-scale motions of sufficient velocities are quickly transformed into small-scale motions via the turbulent cascade, where kinetic energy is dissipated into heat again. Given a weak magnetic seed field, the induction mechanism provides a way of converting motions into magnetic energy by inducing currents. The properties of these motions are crucial in the dynamo mechanism, as well as the environment of the system. The induced currents will lead to a loss of magnetic energy via Joule dissipation. The characteristics of this energy budget (Fig. 2.1)

[1]Common usage is to call $\boldsymbol{B}$ the magnetic field. In this work I will do so as well, although strictly speaking the magnetic field is $\boldsymbol{H}$ and $\boldsymbol{B}$ is the magnetic flux density.

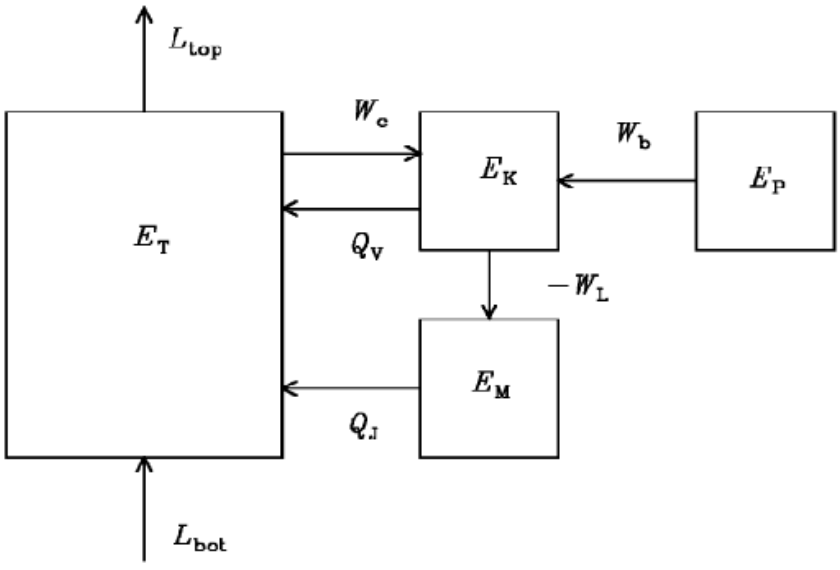

Figure 2.1: Energy budget for e.g. the solar dynamo (Brandenburg and Subramanian, 2005). The thermal energy $E_{\rm T}$ is supplied from the solar interior in form of radiation ($L_{\rm bot}$), which heats the convection zone. Thermal radiation $L_{\rm top}$ at the Sun's surface provides a sink of energy, which balances $L_{\rm bot}$ in global thermal equilibrium. Buoyancy $W_{\rm C}$ cools the system down by creating motions $E_{\rm K}$, which are resistively dissipated ($Q_{\rm V}$). The Lorentz force $W_{\rm L}$ is responsible for transforming kinetic into magnetic energy $E_{\rm M}$, which decays resistively via Joule heating $Q_{\rm J}$. In the case of accretion discs also the potential energy $E_{\rm P}$ plays an important role.

strongly depend on various parameters and boundary conditions. Some of the magnetic energy can be in the form of large-scale magnetic fields, and their dynamics is probably best understood in the framework of mean-field theory.

2.2.1 Mean-Field Theory

As there is a clear separation of scales between the observed magnetic fields and the turbulent motions they can be treated as own entities, while any interaction between them might be determining for the dynamo process. In mean-field theory (Steenbeck et al., 1966; Krause and Rädler, 1971; Krause and Rädler, 1980) only the evolution of the mean quantities is considered, where every field $\boldsymbol{B}$ is split into its mean $\overline{\boldsymbol{B}}$ and fluctuating part $\boldsymbol{b}$ like

$$\boldsymbol{B} = \overline{\boldsymbol{B}} + \boldsymbol{b}. \tag{2.6}$$

How the mean $\overline{\boldsymbol{B}}$ is computed is not relevant, as long as it satisfies the Reynolds rules:

$$\overline{\overline{\boldsymbol{B}}_1+\overline{\boldsymbol{B}}_2}=\overline{\boldsymbol{B}}_1+\overline{\boldsymbol{B}}_2, \quad \overline{\overline{\boldsymbol{B}}}=\overline{\boldsymbol{B}}, \quad \overline{\boldsymbol{b}}=0 \tag{2.7}$$

$$\overline{\overline{\boldsymbol{B}}_1\overline{\boldsymbol{B}}_2}=\overline{\boldsymbol{B}}_1\overline{\boldsymbol{B}}_2, \quad \overline{\overline{\boldsymbol{B}}\boldsymbol{b}}=0, \quad \overline{\partial_\mu\overline{\boldsymbol{B}}}=\partial_\mu\overline{\boldsymbol{B}}, \qquad \mu=0,1,2,3. \tag{2.8}$$

Commonly, averages over one or two spatial coordinates are taken for the mean fields, e.g.

$$\overline{\boldsymbol{B}}(z,t)=\int \boldsymbol{B}(\boldsymbol{x},t)\,\mathrm{d}x\,\mathrm{d}y. \tag{2.9}$$

What happens on scales of the turbulent motions which are not resolved, has to be modeled in a way which strongly depends on the problem. Transport coefficients then incorporate any effects coming from the small-scale fields and affect the mean fields. They directly appear in the evolution equations for the large-scale fields. Any back reaction from the large to the small scales does not need to be excluded. In modern mean-field models such back reactions are modeled by providing evolution equations for the transport coefficients together with the mean-fields.

The mean-field form of the induction equation (2.1) is easily obtained by applying the Reynolds rules:

$$\partial_t\overline{\boldsymbol{B}}=\eta\nabla^2\overline{\boldsymbol{B}}+\boldsymbol{\nabla}\times(\overline{\boldsymbol{U}}\times\overline{\boldsymbol{B}}+\overline{\boldsymbol{\mathcal{E}}}), \quad \boldsymbol{\nabla}\cdot\overline{\boldsymbol{B}}=0, \tag{2.10}$$

with the electromotive force (EMF) $\boldsymbol{\mathcal{E}}=\boldsymbol{u}\times\boldsymbol{b}$.

In order to dispose of fluctuating quantities in the EMF, it has to be modeled via the mean-fields. Which mean-field quantities are used depends on the relevant physics of the system, e.g. whether it is a rotating system. The from of $\boldsymbol{\mathcal{E}}$ also depends on whether or not the system is isotropic. Probably the simplest form is by making $\boldsymbol{\mathcal{E}}$ dependent only on the mean magnetic field $\overline{\boldsymbol{B}}$ (Steenbeck et al., 1966):

$$\mathcal{E}_i(\boldsymbol{x},t)=\mathcal{E}_i^{(0)}(\boldsymbol{x},t)+\int\int K_{ij}(\boldsymbol{x},\boldsymbol{x}',t,t')\overline{B}_j(\boldsymbol{x}-\boldsymbol{x}',t-t')\,\mathrm{d}^3x'\,\mathrm{d}t', \tag{2.11}$$

with the Einstein summation convention for double indices and the integration kernel $K_{ij}(\boldsymbol{x},\boldsymbol{x}',t,t')$. A Taylor expansion for $\overline{\boldsymbol{B}}$ simplifies its form to

$$\mathcal{E}_i=\alpha_{ij}\overline{B}_j+b_{ijk}\frac{\partial\overline{B}_j}{\partial x_k}+\ldots, \tag{2.12}$$

where it is also assumed that $\overline{\boldsymbol{B}}$ affects the EMF only instantaneously and locally. The coefficients are then integrals of the kernel:

$$\alpha_{ij} = \int\int K_{ij}(\boldsymbol{x},\boldsymbol{x}',t,t')\,\mathrm{d}^3x'\,\mathrm{d}t', \tag{2.13}$$

$$b_{ijk} = \int\int K_{ij}(\boldsymbol{x},\boldsymbol{x}',t,t')(x_k'-x_k)\,\mathrm{d}^3x'\,\mathrm{d}t'. \tag{2.14}$$

For homogeneous and isotropic systems the EMF attains the often used form

$$\mathcal{E} = \alpha \overline{\boldsymbol{B}} - \eta_{\mathrm{t}} \boldsymbol{\nabla} \times \overline{\boldsymbol{B}}, \tag{2.15}$$

$$\alpha_{ij} = \alpha \delta_{ij}, \tag{2.16}$$

$$b_{ijk} = \eta_{\mathrm{t}} \varepsilon_{ijk}, \tag{2.17}$$

with the turbulent magnetic diffusivity $\eta_{\mathrm{t}} \approx u_{\mathrm{rms}}/(3k_{\mathrm{f}})$, where u_{rms} is the root mean square of the velocity and k_{f} the inverse length scale of the turbulence. Combining equation (2.15) with the mean-field induction equation (2.10) leads to the induction equation for the mean magnetic field

$$\frac{\partial \overline{\boldsymbol{B}}}{\partial t} = \boldsymbol{\nabla} \times (\alpha \overline{\boldsymbol{B}}) + \eta_{\mathrm{T}} \nabla^2 \overline{\boldsymbol{B}}, \tag{2.18}$$

where $\eta_{\mathrm{T}} = \eta + \eta_{\mathrm{t}}$ is the total magnetic diffusivity, which has been assumed to be constant. It is readily clear that, given an initial seed magnetic field of any strength, the presence of α will enhance $\overline{\boldsymbol{B}}$, which leads to its exponential growth. A back reaction of $\overline{\boldsymbol{B}}$ on α is needed in order to stop the growth and make the field saturate. The form of α and its characteristics during saturation is discussed in section 2.2.2.

2.2.2 The α Effect

Modeling the form of α varies depending on the physical system. One of the simplest forms reads (Moffatt, 1978; Krause and Rädler, 1980)

$$\alpha = \alpha_{\mathrm{K}} = -\tau \overline{\boldsymbol{\omega} \cdot \boldsymbol{u}}/3, \tag{2.19}$$

with the small-scale vorticity $\boldsymbol{\omega} = \boldsymbol{\nabla} \times \boldsymbol{u}$ and the correlation time of the turbulence $\tau \approx 1/(u_{\mathrm{rms}} k_{\mathrm{f}})$. This implies that small-scale helical motions $\boldsymbol{u}$ are responsible for the exponential growth of the large-scale magnetic field $\overline{\boldsymbol{B}}$.

Without any quenching mechanism $\overline{\boldsymbol{B}}$ would grow indefinitely. A back reaction of $\overline{\boldsymbol{B}}$ on α when the system is close to equipartition is necessary. The algebraic quenching forms

$$\alpha = \alpha_{\mathrm{K}} (1 - \overline{\boldsymbol{B}}^2 / B_{\mathrm{eq}}^2), \quad (\overline{\boldsymbol{B}}^2 \ll B_{\mathrm{eq}}^2), \tag{2.20}$$

with the equipartition field strength B_{eq} and

$$\alpha = \frac{\alpha_{\mathrm{K}}}{1 + \overline{\boldsymbol{B}}^2 / B_{\mathrm{eq}}^2} \tag{2.21}$$

were introduced heuristically by Roberts and Soward (1975) and Ivanova and Ruzmaikin (1977), respectively. The dynamics of magnetized media strongly

depends on the magnetic Reynolds number

$$\mathrm{Re_M} = \frac{u_{\mathrm{rms}}}{\eta k_{\mathrm{f}}}. \tag{2.22}$$

Based on simulations, Vaĭnshteĭn and Cattaneo (1992) discovered the importance of the magnetic Reynolds number for the quenching. The resulting quenching is similar to equation (2.21)

$$\alpha = \frac{\alpha_{\mathrm{K}}}{1 + \mathrm{Re_M}\overline{\boldsymbol{B}}^2/B_{\mathrm{eq}}^2} \tag{2.23}$$

and is called catastrophic α quenching, because for the Sun $\mathrm{Re_M} \approx 10^9$ and galaxies $\mathrm{Re_M} \approx 10^{15}$, so α would be too small to be meaningful for even $|\overline{\boldsymbol{B}}| \ll B_{\mathrm{eq}}$.

The construction of α provided by equation (2.19) did not take into account the conservation of magnetic helicity, which is true for astrophysical systems and dynamically relevant times. Under this constraint the total α (Pouquet et al., 1976) is

$$\alpha = \alpha_{\mathrm{K}} + \alpha_{\mathrm{M}} = -\tau\overline{\boldsymbol{\omega}\cdot\boldsymbol{u}}/3 + \tau\overline{\boldsymbol{j}\cdot\boldsymbol{b}}/(3\overline{\rho}). \tag{2.24}$$

So it is composed of the kinetic α_{K} and magnetic α_{M}. The presence of current helicity α_{M} will reduce α and provide an efficient quenching mechanism, which proves to be also dependent on the magnetic Reynolds number $\mathrm{Re_M}$ (see section 2.2.4). As α_{M} grows it will balance α_{K} and the dynamo saturates. For a system in a steady state equation (2.23) can be regained if the mean current density vanishes (Brandenburg and Subramanian, 2005).

2.2.3 α^2 Dynamo

In absence of any mean velocity field $\overline{\boldsymbol{U}}$ the growth of the dynamo is purely powered by the α effect. The induction equation for the mean magnetic field has the simple form of equation (2.18). As long as the mean magnetic field is so small that the Lorentz force does not provide any significant back reaction on the fluid, equation (2.18) can be linearized. One can search for solutions of the form

$$\overline{\boldsymbol{B}}(t) = \Re\left(\hat{\boldsymbol{B}}(k)\exp(\mathrm{i}\boldsymbol{k}\cdot\boldsymbol{x} + \lambda t)\right), \tag{2.25}$$

which results in the eigenvalue problem

$$\lambda\hat{\boldsymbol{B}}(k) = \begin{pmatrix} -\eta_{\mathrm{T}}k^2 & -\mathrm{i}\alpha k_z & \mathrm{i}\alpha k_y \\ \mathrm{i}\alpha k_z & -\eta_{\mathrm{T}}k^2 & -\mathrm{i}\alpha k_x \\ -\mathrm{i}\alpha k_y & \mathrm{i}\alpha k_x & -\eta_{\mathrm{T}}k^2 \end{pmatrix}\hat{\boldsymbol{B}}(k), \tag{2.26}$$

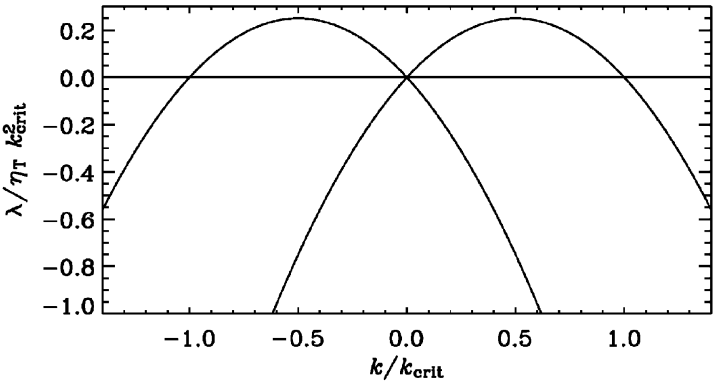

Figure 2.2: Dispersion relation for the mean-field α^2 dynamo, with the growth rate λ in dependence of the wave number. The critical wave number for dynamo action is $k_{\rm crit} = \alpha/\eta_{\rm T}$ (Brandenburg and Subramanian, 2005).

with the eigenvectors $\hat{\boldsymbol{B}}(k)$ and growth rates (roots) λ (Moffatt, 1978)

$$\lambda_0 = -\eta_{\rm T} k^2, \quad \lambda_\pm = -\eta_{\rm T} k^2 \pm |\alpha k|. \tag{2.27}$$

Depending on the value of α different modes get more or less strongly excited. The strongest excited mode is for $k_{\rm max} = \pm\alpha/(2\eta_{\rm T})$ (Fig. 2.2).

Injection of small-scale kinetic helicity leads to the creation of helical small-scale magnetic fields. Since the total magnetic helicity has to be conserved, a helical large-scale field arises with opposite helicity. As time evolves, the scale of the mean field becomes larger (Frisch et al., 1975; Léorat et al., 1975) until it reaches the size of the system. At the end of the saturation the magnetic energy spectrum shows two characteristic humps, one at the forcing scale, i.e. the scale of the turbulent motion, and another at the scale of the system (Brandenburg, 2001).

2.2.4 Magnetic Helicity Conservation

Magnetic helicity conservation is a crucial aspect for the saturation behavior of the large-scale magnetic field in dynamos. Astrophysically relevant cases for which helicity is conserved are closed systems and systems in which fluxes of helicity are so small that they are irrelevant on the time scales of interest. The presence of magnetic helicity not only slows down the saturation of the mean magnetic field, but also determines its saturation amplitude.

For a closed system the evolution equation of the mean magnetic helicity is

$$\frac{\rm d}{{\rm d}t} H'_{\rm M} = \frac{\rm d}{{\rm d}t} \langle \boldsymbol{A} \cdot \boldsymbol{B} \rangle = -2\eta \langle \boldsymbol{J} \cdot \boldsymbol{B} \rangle, \tag{2.28}$$

where $\langle . \rangle$ denote volume averages. In the steady state $H'_{\rm M}$ does not change in time. Splitting the field in mean and fluctuating parts results in the steady state condition

$$\langle \overline{\boldsymbol{J}} \cdot \overline{\boldsymbol{B}} \rangle = -\langle \boldsymbol{j} \cdot \boldsymbol{b} \rangle. \tag{2.29}$$

For a helically driven system the magnetic field and current density are partially helical:

$$\boldsymbol{\nabla} \times \overline{\boldsymbol{B}} = \pm \varepsilon_{\rm m} k_{\rm m} \overline{\boldsymbol{B}}, \qquad \boldsymbol{\nabla} \times \boldsymbol{b} = \mp \varepsilon_{\rm f} k_{\rm f} \boldsymbol{b}, \tag{2.30}$$

with the wave numbers of the small and large scales, $k_{\rm m}$ and $k_{\rm f}$, and the fractional helicities $\varepsilon_{\rm m}$ and $\varepsilon_{\rm f}$. The different signs in $\overline{\boldsymbol{B}}$ and $\boldsymbol{b}$ come from total current helicity conservation Eq. (2.29), which causes the helically driven dynamo to create helicities of opposite sign in the large and small scales. From equation (2.30) we obtain

$$\langle \overline{\boldsymbol{J}} \cdot \overline{\boldsymbol{B}} \rangle = \pm \varepsilon_{\rm m} k_{\rm m} \langle \overline{\boldsymbol{B}}^2 \rangle, \qquad \langle \boldsymbol{j} \cdot \boldsymbol{b} \rangle = \mp \varepsilon_{\rm f} k_{\rm f} \langle \boldsymbol{b}^2 \rangle. \tag{2.31}$$

Hence in the steady state we have

$$\langle \overline{\boldsymbol{B}}^2 \rangle = \frac{\varepsilon_{\rm m} k_{\rm f}}{\varepsilon_{\rm f} k_{\rm m}} \langle \boldsymbol{b}^2 \rangle. \tag{2.32}$$

Or for the fully helical case, i.e. $\varepsilon_{\rm m} = \varepsilon_{\rm f} = 1$:

$$\langle \overline{\boldsymbol{B}}^2 \rangle = \frac{k_{\rm f}}{k_{\rm m}} \langle \boldsymbol{b}^2 \rangle. \tag{2.33}$$

As the separation of scales $k_{\rm f}/k_{\rm m}$ increases, the saturation strength of the mean magnetic field increases with respect to the small-scale field. The conservation of magnetic helicity slows down the saturation of the mean magnetic field. The time which is needed to reach this state is dictated by the magnetic resistivity. Close to saturation the small- and large-scale current helicities cancel (see equation (2.28)). The current helicities can be expressed in terms of the magnetic helicity

$$\langle \overline{\boldsymbol{J}} \cdot \overline{\boldsymbol{B}} \rangle = k_{\rm m}^2 \langle \overline{\boldsymbol{A}} \cdot \overline{\boldsymbol{B}} \rangle, \tag{2.34}$$

$$\langle \boldsymbol{j} \cdot \boldsymbol{b} \rangle = k_{\rm f}^2 \langle \boldsymbol{a} \cdot \boldsymbol{b} \rangle. \tag{2.35}$$

The small-scale magnetic field saturates with the end of the kinematic phase. This means that $\langle \boldsymbol{j} \cdot \boldsymbol{b} \rangle$ is approximately constant, but $\langle \overline{\boldsymbol{A}} \cdot \overline{\boldsymbol{B}} \rangle$ is not, so one neglects the time derivative of the small-scale magnetic helicity in equation (2.28), which for the steady state means

$$\frac{\mathrm{d}}{\mathrm{d}t} H'_{\rm M} \approx \frac{\mathrm{d}}{\mathrm{d}t} \langle \overline{\boldsymbol{A}} \cdot \overline{\boldsymbol{B}} \rangle = -2\eta k_{\rm m}^2 \langle \overline{\boldsymbol{A}} \cdot \overline{\boldsymbol{B}} \rangle - 2\eta k_{\rm f}^2 \langle \boldsymbol{a} \cdot \boldsymbol{b} \rangle, \tag{2.36}$$

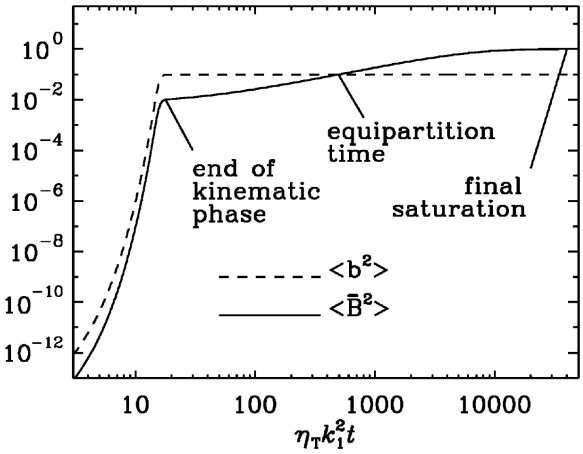

Figure 2.3: Time evolution of the mean magnetic energy $\langle \overline{\boldsymbol{B}}^2 \rangle$ and the energy in the small-scale fields $\langle \boldsymbol{b}^2 \rangle$ for an α^2 dynamo. The small-scale field grows exponentially and saturates within dynamical times. The large-scale field grows exponentially as well, after which its growth is dominated by the magnetic resistivity, which means a long resistive saturation phase (Brandenburg and Dobler, 2002).

which has the solution

$$\langle \overline{\boldsymbol{A}} \cdot \overline{\boldsymbol{B}} \rangle(t) = \langle \boldsymbol{a} \cdot \boldsymbol{b} \rangle(t) \frac{k_\mathrm{f}^2}{k_\mathrm{m}^2} \left(1 - e^{-2\eta k_\mathrm{m}^2 (t - t_\mathrm{sat})} \right). \tag{2.37}$$

As long as the dynamical time scale is much shorter than the resistive time scale, which for physically relevant problems is mostly the case, the small-scale magnetic helicity $\langle \boldsymbol{a} \cdot \boldsymbol{b} \rangle$ can be considered time independent close to saturation. For the mean magnetic field this means

$$\langle \overline{\boldsymbol{B}}^2 \rangle(t) = \langle \boldsymbol{b}^2 \rangle \frac{\varepsilon_\mathrm{f} k_\mathrm{f}}{\varepsilon_\mathrm{m} k_\mathrm{m}} \left(1 - e^{-2\eta k_\mathrm{m}^2 (t - t_\mathrm{sat})} \right). \tag{2.38}$$

The saturation time of the mean magnetic field, therefore, depends on the magnetic resistivity η (Fig. 2.3) as

$$\tau = (2\eta k_\mathrm{m}^2)^{-1}. \tag{2.39}$$

Astrophysical systems have such low values for η that τ exceeds the age of the object or even the age of the Universe. The most promising way to reduce the saturation time is by allowing for magnetic helicity fluxes (Blackman and Field, 2000; Kleeorin et al., 2000) as they are discussed in **Paper II**.

2.3 Gauge Freedom for Magnetic Helicity

Magnetic helicity is defined with the magnetic vector potential $\boldsymbol{A}$. For any potential there exists the freedom of choosing a gauge. The magnetic field $\boldsymbol{B}$ in terms of its vector potential $\boldsymbol{A}$ is $\boldsymbol{B} = \boldsymbol{\nabla} \times \boldsymbol{A}$. Adding the gradient of a scalar field ϕ to $\boldsymbol{A}$ does not change $\boldsymbol{B}$:

$$\boldsymbol{B}' = \boldsymbol{\nabla} \times (\boldsymbol{A} + \boldsymbol{\nabla}\phi) = \boldsymbol{\nabla} \times \boldsymbol{A} = \boldsymbol{B}, \tag{2.40}$$

since $\boldsymbol{\nabla} \times \boldsymbol{\nabla}\phi = 0$. Commonly used gauges include the Coulomb gauge, where $\boldsymbol{\nabla} \cdot \boldsymbol{A} = 0$, and the resistive gauge where the induction equation for $\boldsymbol{A}$ reads

$$\frac{\partial \boldsymbol{A}}{\partial t} = \boldsymbol{U} \times \boldsymbol{B} + \eta \boldsymbol{\nabla}^2 \boldsymbol{A}. \tag{2.41}$$

With the gauge freedom magnetic helicity density can change as well:

$$\boldsymbol{A} \cdot \boldsymbol{B} \rightarrow \boldsymbol{A} \cdot \boldsymbol{B} + \boldsymbol{\nabla}\phi \cdot \boldsymbol{B}. \tag{2.42}$$

Total magnetic helicity is in general gauge dependent too:

$$\int \boldsymbol{A} \cdot \boldsymbol{B} \, \mathrm{d}V \quad \rightarrow \quad \int \boldsymbol{A}' \cdot \boldsymbol{B} \, \mathrm{d}V + \int \boldsymbol{\nabla}\phi \cdot \boldsymbol{B} \, \mathrm{d}V \tag{2.43}$$

$$= \quad \int \boldsymbol{A}' \cdot \boldsymbol{B} \, \mathrm{d}V + \int_F \phi \boldsymbol{B} \cdot \, \mathrm{d}\boldsymbol{f}, \tag{2.44}$$

where at the last step Gauss' theorem was used to transform the volume integral into a surface integral with surface normal $\boldsymbol{f}$. As long as the component of $\boldsymbol{B}$ normal to the bounding surface vanishes the magnetic helicity is gauge independent. Alternatively, periodic boundary conditions have the same result. Fluxes of magnetic helicity are gauge dependent too. From equation (2.1) the magnetic helicity flux can be derived as

$$\boldsymbol{F}_h = \boldsymbol{A} \times (\boldsymbol{U} \times \boldsymbol{B}) + \eta \boldsymbol{\nabla}\phi \times \boldsymbol{J}. \tag{2.45}$$

A gauge-invariant definition of the magnetic helicity is the relative magnetic helicity (Berger and Field, 1984). It is relative to a reference field $\boldsymbol{B}^{\mathrm{ref}} = \boldsymbol{\nabla} \times \boldsymbol{A}^{\mathrm{ref}}$:

$$H_{\mathrm{rel}} = \int (\boldsymbol{A} + \boldsymbol{A}^{\mathrm{ref}}) \cdot (\boldsymbol{B} - \boldsymbol{B}^{\mathrm{ref}}) \, \mathrm{d}V, \tag{2.46}$$

with $\boldsymbol{B}^{\mathrm{ref}} = \boldsymbol{\nabla}\phi$ and the boundary condition $\hat{\mathbf{n}} \cdot \boldsymbol{B}^{\mathrm{ref}} = \hat{\mathbf{n}} \cdot \boldsymbol{B}$, where $\hat{\mathbf{n}}$ is the normal vector at the surface.

Physically the gauge choice has no effect on the dynamics. On the other hand it will be shown that the presence of magnetic helicity fluxes does affect the evolution of the dynamo. In **Paper III** and **Paper IV** this apparent contradiction will be addressed.

2.4 Magnetic Field Relaxation and Stability

2.4.1 Relaxed States

Freely decaying magnetic fields try to develop a state of minimal magnetic energy. The evolution is, however, restricted. The presence of conserved quantities, most notably the magnetic helicity, constitute severe constraints. Finding the minimum of the magnetic energy under the constraint of constant magnetic helicity is a simple variational problem first investigated by Woltjer (1958). The resulting magnetic field obeys

$$\boldsymbol{\nabla} \times \boldsymbol{B} = \alpha \boldsymbol{B}, \tag{2.47}$$

with constant α, thus constitutes a linear force-free field.

A more restrictive constraint was used by Taylor (1974), where the magnetic helicity along each field line has to be conserved. For an ergodic field, where one field line fills the whole space, the two restrictions are equivalent. For laboratory fields confined in tori, however, ergodic field lines may not necessarily exist. Instead one can think of a finite or infinite set of distinct field lines. In that case the minimal energy state is a non-linear force-free state

$$\boldsymbol{\nabla} \times \boldsymbol{B} = \lambda(a,b) \boldsymbol{B}, \tag{2.48}$$

with $\lambda(a,b)$ varying between field lines, which are parameterized by a and b.

2.4.2 Frozen-in Magnetic Fields

For astrophysical objects magnetic resistivity is small enough, such that on dynamically relevant time scales the magnetic field can be considered frozen into the fluid (Batchelor, 1950; Priest and Forbes, 2000). Any magnetic field is transported with the fluid. This implies that the magnetic flux through any surface C does not change, since both fluid and magnetic field move jointly (Fig. 2.4). Flux freezing is a concept used in both, the flux transport dynamos (Choudhuri et al., 1995; Charbonneau et al., 1999) and the enhancements of magnetic energy via the stretch, twist and fold mechanism (Vaĭnshteĭn and Zel'dovich, 1972; Priest and Forbes, 2000).

2.4.3 Realizability Condition

The presence of magnetic helicity has important implications for the stability of the field. For a non-zero helicity spectrum $H_{\mathrm{M}}(k)$, the lowest value of the spectral magnetic energy $E_{\mathrm{M}}(k)$ that can be attained is given by the *realizability condition* (Arnold, 1974; Moffatt, 1978)

$$E_{\mathrm{M}}(k) \geq k|H_{\mathrm{M}}(k)|/2. \tag{2.49}$$

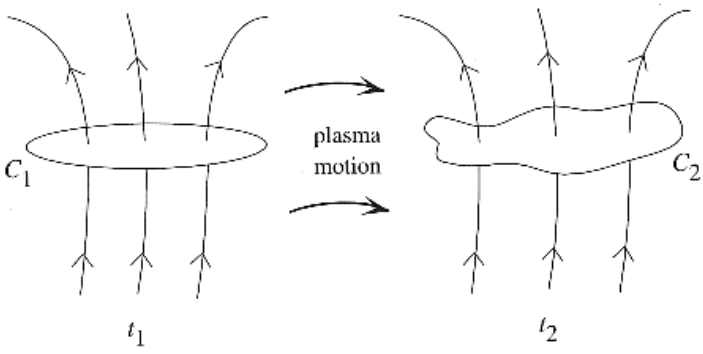

Figure 2.4: As the fluid evolves the surface C_1 gets distorted into the shape C_2. Because the magnetic field is frozen in for low magnetic resistivity the magnetic flux through surface C_2 is unchanged (Priest and Forbes, 2000, p. 24).

Together with the spectral magnetic energy $E_{\mathrm{M}}(k)$ also the total magnetic energy is bound by

$$E_{\mathrm{M}} \geq \int k|H_{\mathrm{M}}(k)|/2 \, \mathrm{d}k. \tag{2.50}$$

In that context the minimum value for the correlation length can be defined as (Tevzadze et al., 2012)

$$l_{\mathrm{corr}}^{\mathrm{min}} = |H_{\mathrm{M}}|/(2E_{\mathrm{M}}). \tag{2.51}$$

2.4.4 Topological Interpretation

A colorful interpretation of magnetic helicity is the mutual linkage of magnetic field lines. For instance two magnetic field lines can be linked into each other once (Fig. 1.3) or several times. The number of mutual linkage, i.e. the number the tubes wind around each other, is directly proportional to the total magnetic helicity (Moffatt, 1969; Moffatt and Ricca, 1992)

$$H_{\mathrm{M}} = \int_V \boldsymbol{A} \cdot \boldsymbol{B} \, \mathrm{d}V = 2n\phi_1\phi_2, \tag{2.52}$$

with the magnetic fluxes ϕ_1 and ϕ_2 through the magnetic field lines and the number of mutual linkage n. The picture also works for flux tubes with finite width but without internal twist or self-linking.

With this picture of magnetic helicity the realizability condition can be interpreted as the reluctance of the field to brake its field lines and change its topology. Hence the magnetic field provides a topological invariant, which not only qualifies the configuration (helical/non-helical), but even gives a quantitative measure for the linking of the field.

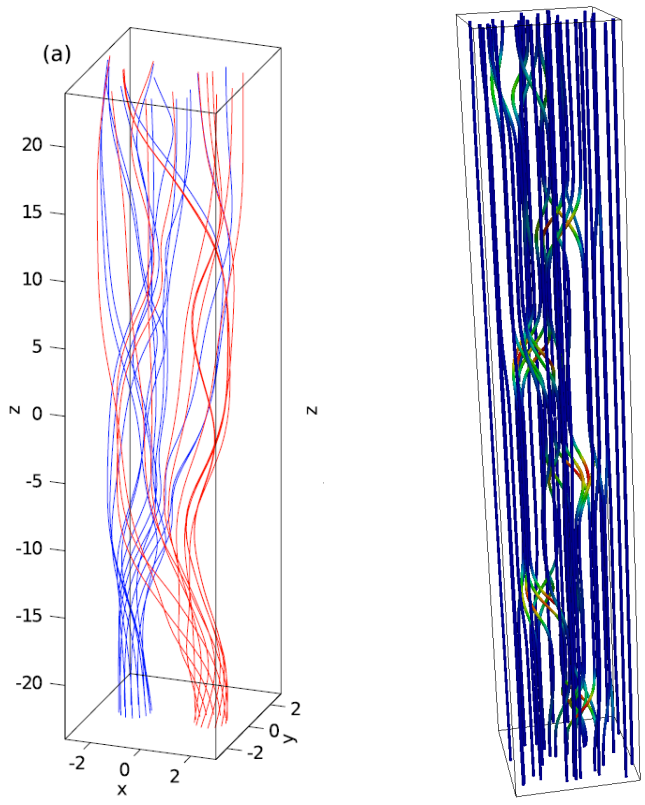

Figure 2.5: Magnetic field lines for the configuration used by Yeates et al. (2010) corresponding to the color mapping in Fig. 2.7.

2.4.5 Topology Beyond Magnetic Helicity

Magnetic helicity is not the only topological quantity which is conserved for low magnetic resistivity. Invariants of order three and four in the magnetic field were suggested by Ruzmaikin and Akhmetiev (1994), which are non-zero for field configurations without magnetic helicity, which makes them intriguing quantities to test decay properties with. The practical usage is, however, limited since they are defined for separate flux tubes and have not been expressed for arbitrary fields, like the linking number for magnetic helicity.

A more practical topological invariant, which is conserved for low magnetic diffusivity, is the fixed points index (see, e.g., Yeates et al. (2010)). It is defined for fields with a preferential direction, like toroidal tokamak fields or fields with a positive component in the z-direction (Fig. 2.5).

For such fields a mapping $(x,y) \rightarrow \boldsymbol{F}(x,y)$ can be defined between two surfaces, where the field lines start and end. Fixed points are those values for

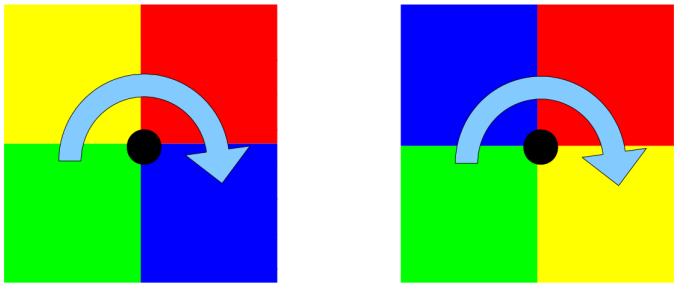

Figure 2.6: Neighborhood of fixed points with different color mappings. The left fixed point has positive sign, while the right has negative sign.

(x,y) for which the mapping is onto itself, i.e. $\boldsymbol{F}(x,y) = (x,y)$. They are signed and can be either $+1$ or -1. For a continuous mapping there is a neighborhood for each fixed point in which it is the only fixed point. Further, there exist points in this neighborhood for which the following inequalities hold:

$$F_x > x, \quad F_y > y, \tag{2.53}$$
$$F_x < x, \quad F_y > y, \tag{2.54}$$
$$F_x < x, \quad F_y < y, \tag{2.55}$$
$$F_x > x, \quad F_y < y. \tag{2.56}$$

Assigning a different color for each case gives the field line mapping of the field. The sign results from the sequence of the colors (Fig. 2.6). The sum over all fixed points gives the fixed point index, which is a conserved quantity in low resistivity MHD (Brown, 1971):

$$T = \sum_i t_i, \tag{2.57}$$

with the sign of the ith fixed point t_i.

Even for simple magnetic fields (Fig. 2.5, right panel) the color mapping can be complex (Fig. 2.7, left panel). The complexity comes about in a similar fashion as in the two-dimensional stirring in fluids (Boyland et al., 2000), where stirring corresponds to braiding of field lines. The number of initial fixed points for the configuration in Fig. 2.5 (right panel) is 26. The fixed points index, however, is 2. After resistive time evolution fixed points of opposite signs merge, while the fixed point index is conserved (Fig. 2.7, right panel).

The conservation of the fixed point index imposes an additional constraint in magnetic field relaxation. In practice it turns out that the field does not reach the Taylor state and retains higher energies.

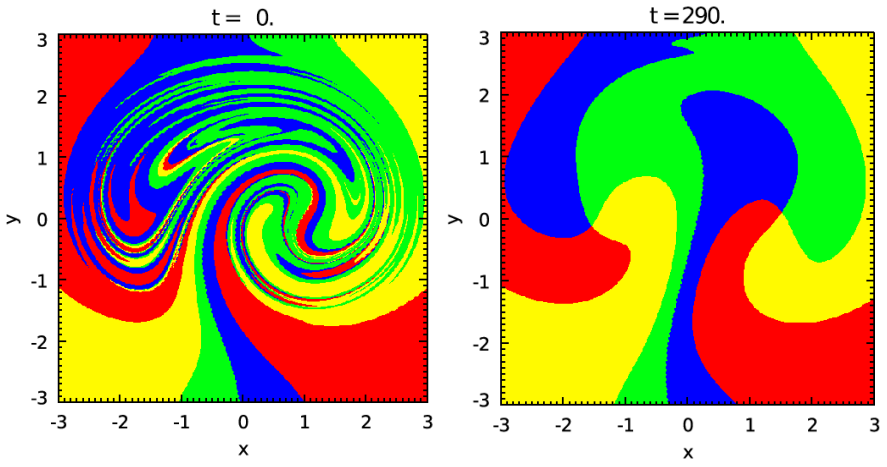

Figure 2.7: Color mapping for the configuration illustrated in Fig. 2.5 at initial time (left) and after some time evolution (right) (Yeates et al., 2010).

2.5 Observing Helical Magnetic Fields

The gauge dependence of magnetic helicity density makes it difficult to measure it directly. As a proxy the current helicity $\boldsymbol{J} \cdot \boldsymbol{B}$ is often used (Yeates et al., 2008). Its measurement is still not easy, since only recently all three components of $\boldsymbol{B}$ could be measured at the solar surface. Prior to that, force-free assumptions were used for field line extrapolation (Gibson et al., 2002).

For helical large-scale structures no direct measurements of $\boldsymbol{B}$ are necessary to infer the helical nature of magnetic fields on, e.g., the Sun's surface. Emerging coronal loops often carry hot plasma with them, which is trapped in the magnetic flux tubes. The plasma can only move along the field lines due to strong Lorentz forces (Fig. 2.8). Often those loops show a pig tail like shape, which suggests large-scale magnetic helicity. Force-free extrapolations support the observation of twisted magnetic loops (Fig. 2.9). The force free assumption is, however, only valid at heights of 400 km and above the photosphere (Metcalf et al., 1995), which casts some doubt on such extrapolations, although they reproduce the loops observed in X-ray observations.

Helical structures have implications for the dynamics of the Sun's plasma. It has been shown that N- and S-shaped helical regions are more likely to result in coronal mass ejections (Canfield et al., 1999). The Sun, therefore, possibly sheds magnetic helicity, which has far reaching implications for the dynamo mechanism.

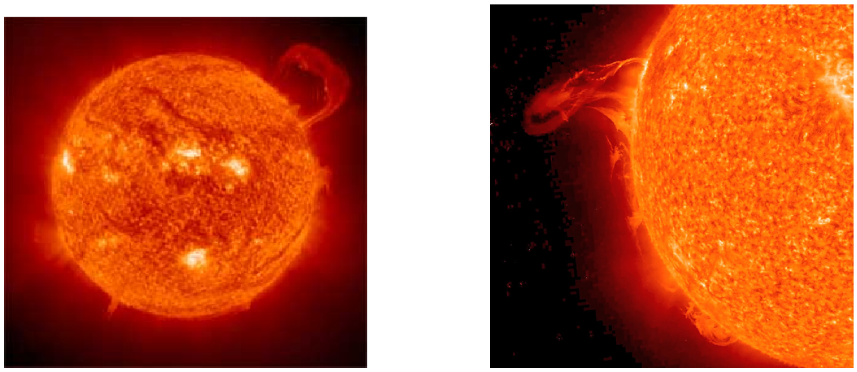

Figure 2.8: SOHO observations of coronal mass ejections. The image to the right was taken in May 7 2010.

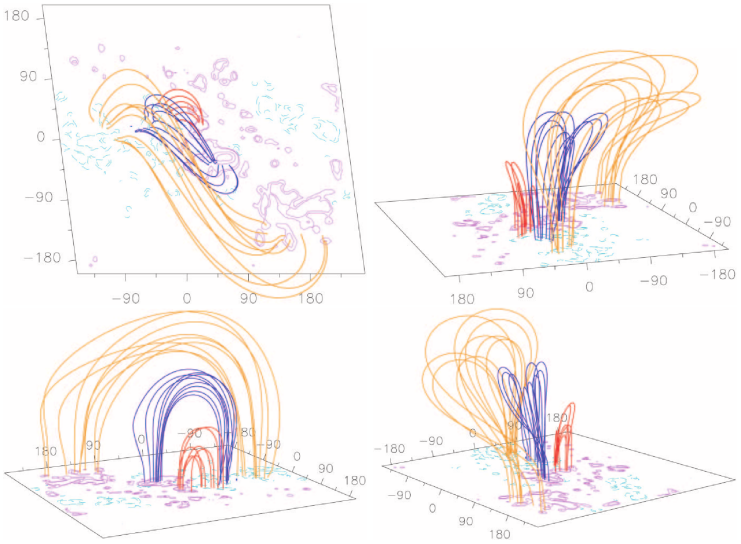

Figure 2.9: Force-free extrapolation of the Sun's surface magnetic field from data taken August 21 1999 (Gibson et al., 2002).

3. Magnetic Helicity Conservation and Fluxes in Turbulent Dynamos

Do you include turbulence?

popular saying

3.1 Magnetic Helicity Conservation in α^2 Dynamos

For the helically driven α^2 dynamo the growth rate of the different modes depends on the forcing α and the wave number k as (Blackman and Brandenburg, 2002)

$$\lambda = \alpha k - \eta_{\rm T} k^2 = (C_\alpha - 1)\eta_{\rm T} k^2, \tag{3.1}$$

where $C_\alpha = \alpha_{\rm K}/(\eta_{\rm T} k)$ is the dynamo number for the α^2 dynamo. The onset value for dynamo action is obviously at $C_\alpha = 1$. In the limit of high conductivity (Moffatt, 1978; Krause and Rädler, 1980) we have $\alpha_{\rm K} = -(\tau/3)\langle \boldsymbol{\omega} \cdot \boldsymbol{u} \rangle$ and $\eta_{\rm t} = (\tau/3)\langle \boldsymbol{u}^2 \rangle$. This allows us to reformulate the expression for the dynamo coefficient C_α such that it reads

$$C_\alpha = -\frac{\langle \boldsymbol{\omega} \cdot \boldsymbol{u} \rangle}{k \langle \boldsymbol{u}^2 \rangle \iota}, \tag{3.2}$$

with the correction factor $\iota = \eta_{\rm T}/\eta_{\rm t}$. With the normalized helicity for the small-scale field $\varepsilon_{\rm f} = \langle \boldsymbol{\omega} \cdot \boldsymbol{u} \rangle / (k_{\rm f} \langle \boldsymbol{u}^2 \rangle)$ we can write

$$C_\alpha = -\frac{\varepsilon_{\rm f} k_{\rm f}}{k_{\rm m} \iota}. \tag{3.3}$$

The normalized kinetic helicity has to be contrasted with the relative helicity, also called fractional helicity, which is defined in a similar fashion as

$$\tilde{\varepsilon}_{\rm f} = \frac{\langle \boldsymbol{\omega} \cdot \boldsymbol{u} \rangle}{\omega_{\rm rms} u_{\rm rms}}, \tag{3.4}$$

with the root mean square values of the vorticity $\omega_{\rm rms} = \sqrt{\langle \boldsymbol{\omega}^2 \rangle}$ and velocity $u_{\rm rms} = \sqrt{\langle \boldsymbol{u}^2 \rangle}$. From equation (3.3) one sees that the critical value of the normalized helicity for dynamo action scales like $\varepsilon_{\rm f} \propto (k_{\rm f}/k_{\rm m})^{-1}$ with the scale separation ratio $k_{\rm f}/k_{\rm m}$:

$$\varepsilon_{\rm f}^{\rm crit} = \iota \varepsilon_{\rm m} \left(\frac{k_{\rm f}}{k_{\rm m}} \right)^{-1}, \tag{3.5}$$

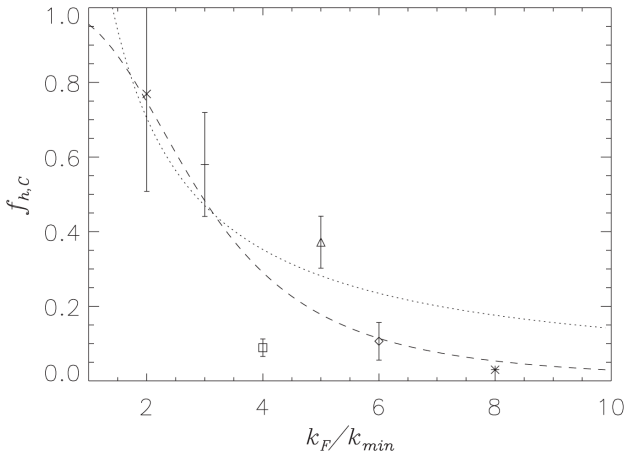

Figure 3.1: Critical values for the fractional helicity f_h in dependence of the scale separation value together with a power law fit (dashed line) and the analytical prediction from mean-field theory given by equation (3.5) (dotted line) (Pietarila Graham et al., 2012).

with the normalized kinetic helicity of the large-scale field

$$\varepsilon_\mathrm{m} = \frac{\langle \overline{\boldsymbol{J}} \cdot \overline{\boldsymbol{B}} \rangle}{k_\mathrm{m} \langle \overline{\boldsymbol{B}}^2 \rangle}. \tag{3.6}$$

Conservation of magnetic helicity still allows for an increase of magnetic helicity at small and large scale if they have opposite signs (Seehafer, 1996; Ji, 1999). In its continuous creation the large scales become even larger (Frisch et al., 1975) until the dynamo saturates with strong magnetic fields in scales of the system size (Blackman and Brandenburg, 2002; Brandenburg et al., 2002). The saturation mean magnetic energy $\overline{B}_\mathrm{sat}$ in dependence of the dynamo number C_α for a closed or periodic system is easily obtained from mean-field theory (Blackman and Brandenburg, 2002):

$$\overline{B}^2_\mathrm{sat}/B^2_\mathrm{eq} = (|C_\alpha| - 1)\, \imath. \tag{3.7}$$

Contrary to this established theory a different scaling was recently found by Pietarila Graham et al. (2012), who predicted a dependence of the form

$$\varepsilon_\mathrm{f}^\mathrm{crit} \propto (k_\mathrm{f}/k_\mathrm{m})^{-3} \tag{3.8}$$

for the critical normalized helicity (Fig. 3.1). The injection of kinetic helicity causes the magnetic field to be helical with magnetic helicity in the small and large scales of opposite sign. As long as the system is closed or periodic, as it is

the case in (Pietarila Graham et al., 2012), the build-up of small-scale magnetic helicity reduces the α effect and the growth of the large-scale magnetic field. In practice this means that after a short exponential growth the mean magnetic field continues growing slowly and saturates on a resistive time scale, which can be large compared to the dynamical time scales for astrophysical systems.

The discrepancy in Pietarila Graham et al. (2012) with the semi analytical predictions from equation (3.3) comes from the method used in determining $C_\alpha^{\rm crit}$. As they only looked at the growth rate of the largest mode at $k = 1$ shortly after the exponential phase at a small fraction of the resistive times, the field will be contaminated by small-scale contributions. The large-scale field becomes dominant at later times when nonlinear effects suppress the small-scale field.

To shed light on this issue, we investigate in **Paper I** the saturation characteristics of a large-scale dynamo in the non-linear regime for a helically driven dynamo in a periodic cube shaped domain, similar to Pietarila Graham et al. (2012). The equations to be solved for this problem are the usual resistive, viscous MHD equations for an isothermal medium:

$$\frac{\partial}{\partial t}\boldsymbol{A} = \boldsymbol{U}\times\boldsymbol{B} - \eta\boldsymbol{J}, \tag{3.9}$$

$$\frac{\mathrm{D}}{\mathrm{D}t}\boldsymbol{U} = -c_{\rm s}^2\boldsymbol{\nabla}\ln\rho + \frac{1}{\rho}\boldsymbol{J}\times\boldsymbol{B} + \boldsymbol{F}_{\rm visc} + \boldsymbol{f}, \tag{3.10}$$

$$\frac{\mathrm{D}}{\mathrm{D}t}\ln\rho = -\boldsymbol{\nabla}\cdot\boldsymbol{U}, \tag{3.11}$$

where the forcing function $\boldsymbol{f}$ is delta correlated in time and provides the energy input. The applied magnetic Reynolds numbers are around 6 in a first set of cases with scale separation values of up to 80. In the latter part we use $\mathrm{Re_M}$ values between 80 and 320 at a scale separation value of $k_{\rm f}/k_{\rm m} = 5$. The magnetic Prandtl number $\mathrm{Pr_M} = \eta/\nu$ is unity if nothing else is stated.

As kinetic energy is injected the magnetic field in both, small- and large-scales grows exponentially during the kinematic phase. Since the system is isotropic, either the *xy*, *xz* or *yz* averaged magnetic field will be dominant (Fig. 3.2), while the other modes die out. Helicity conservation causes the field to saturate slowly on resistive times, which means the magnetic energy M behaves like (Brandenburg, 2001)

$$M(t) = M_0 - M_1 e^{-t/\tau} \tag{3.12}$$

in the resistive phase, where M_0 is the saturation energy and M_1 the initial energy of the simulation run. The resistive time for saturation is given as

$$\tau = (2\eta k_{\rm m}^2)^{-1}. \tag{3.13}$$

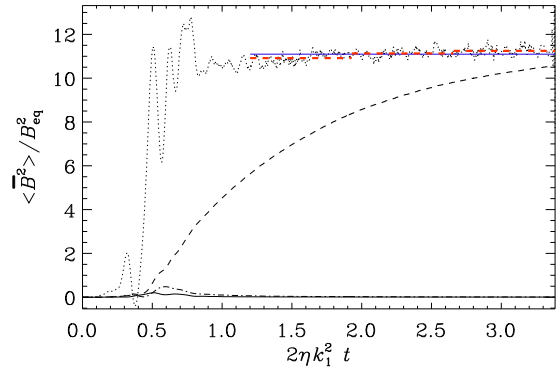

Figure 3.2: Normalized mean magnetic energies in resistive times. The strongest growing mode is the xz average $\langle \boldsymbol{B} \rangle_{xz}$ (dashed line). The xy (solid) and yz (dash-dotted) averages die out. The dotted line represents $\langle \boldsymbol{B}^2 \rangle + \tau \mathrm{d} \langle \boldsymbol{B}^2 \rangle / \mathrm{d}t$, which was used to compute the saturation magnetic field strength without letting the system saturate.

To speed up the calculation of the saturated magnetic field strength a short cut is taken, where the saturation magnetic energy is computed as the time average of

$$\tilde{M}_0(t) = \langle \overline{\boldsymbol{B}}^2 \rangle + \tau \mathrm{d} \langle \overline{\boldsymbol{B}}^2 \rangle / \mathrm{d}t, \tag{3.14}$$

which comes from taking the time derivative of equation (3.12).

For different scale separation ratios and normalized magnetic helicities the mean saturation magnetic energy is determined (Fig. 3.3). As predicted by equation (3.7) the saturation magnetic energy behaves linearly with the dynamo number C_α. Further, the critical value for large-scale dynamo action to start ($C_\alpha^{\mathrm{crit}} = 1$) is approximately reproduced. For the critical value we find $C_\alpha^{\mathrm{crit}} \approx 1.2$, which results in a critical value for the normalized helicity

$$\varepsilon_{\mathrm{f}}^{\mathrm{crit}} \approx 1.2 \iota (k_{\mathrm{f}}/k_{\mathrm{m}})^{-1} = 1.7 (k_{\mathrm{f}}/k_{\mathrm{m}})^{-1}, \tag{3.15}$$

where we use an averaged magnetic Reynolds number that leads to an averaged $\iota \approx 1.41$.

For fixed scale separation ratio, equation (3.7) together with equation (3.3) predict a linear dependence of the saturation energy on the normalized helicity. We plot the normalized magnetic energy for various scale separation ratios in dependence of ε_{f} and make linear fits (Fig. 3.4), from which we can extrapolate the critical values $\varepsilon_{\mathrm{f}}^{\mathrm{crit}} \approx 1.7 (k_{\mathrm{f}}/k_{\mathrm{m}})^{-1}$. The extrapolated values for $\varepsilon_{\mathrm{f}}^{\mathrm{crit}}$ agree well with the theory (Fig. 3.5) and the values extracted from Fig. 3.3.

The theoretical predictions for the closed α^2 dynamo are verified in direct numerical simulations. In order to refute the findings by Pietarila Graham et al. (2012), their parameters have to be accommodated in our investigations.

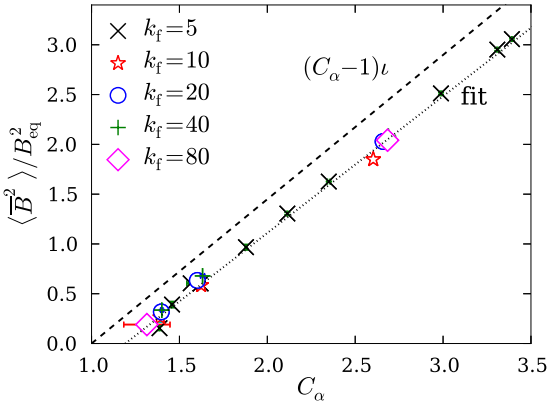

Figure 3.3: Normalized saturation energy of the mean magnetic field in dependence of C_α for various scale separation values. The dashed line is the theoretical prediction given by equation (3.7).

Therefore, high magnetic Reynolds numbers between 80 and 320 are used with magnetic Prandtl numbers 1 and 100. In this case the scale separation ratio is fixed to $k_f/k_m = 5$. The dependence of the normalized magnetic energy (Fig. 3.6, for $\mathrm{Pr_M} = 1$) is shown to behave similarly to the case with $\mathrm{Re_M} = 6$. For higher magnetic Prandtl numbers, however, the slope is higher. This behavior can be explained by different values for the equipartition strength B_{eq}, which is supposed to become smaller for increasing $\mathrm{Pr_M}$, due to the shifted dissipation range. Any different behavior at magnetic Reynolds numbers of 1500, as used by Pietarila Graham et al. (2012), is not to be expected. As a consequence we can refute their findings.

In summary, the theoretical predictions coming from mean-field consideration (equations (3.5) and (3.7)) are well confirmed for the closed α^2 dynamo, which constitutes one of the simplest possible dynamo setups and is often used as reference. The findings by Pietarila Graham et al. (2012) are at variance, most likely because their large-scale dynamo was contaminated by the small-scale dynamo. The present investigation about the non-linear behavior of the large-scale dynamo provides an important confirmation of the general theory.

3.2 Magnetic Helicity Fluxes

The injection of small-scale magnetic helicity causes the small- and large-scale magnetic helicity to grow with opposite sign. The presence of small-scale magnetic helicity $\overline{h}_f = \overline{\boldsymbol{a} \cdot \boldsymbol{b}}$ causes the total α effect to diminish (Gruzinov and Diamond, 1994), such that the growth of the large-scale magnetic field gets quenched (see **Paper I**). Fluxes of this quantity could alleviate this quenching

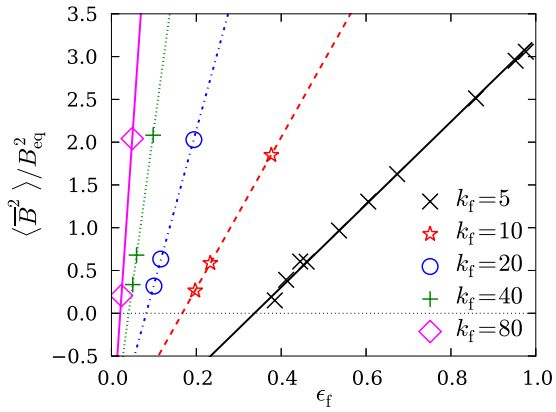

Figure 3.4: Normalized saturation energy of the mean magnetic field in dependence of $\varepsilon_{\rm f}$ for various scale separation values. Equation (3.5) predicts a linear dependence of $\langle \overline{\boldsymbol{B}}^2 \rangle / B_{\rm eq}^2$ on $\varepsilon_{\rm f}$, which is shown in the linear fits (lines).

by reducing its value. There are various ways of creating such fluxes (Kleeorin and Rogachevskii, 1999; Vishniac and Cho, 2001; Subramanian and Brandenburg, 2004). Not all of them help in alleviating catastrophic α quenching. In **Paper II** we discuss the most promising type of flux (Blackman and Field, 2000).

Quenching of the α effect becomes more pronounced as the magnetic Reynolds number increases such that for physically relevant values of $\mathrm{Re_M}$ any large-scale dynamo becomes impossible to drive. That is why it is called catastrophic α quenching. To address the question whether magnetic helicity fluxes have any significant effect on the alleviation of the α quenching mechanism high magnetic Reynolds numbers are required of e.g. 10^5. Such simulations require computational resources, which are currently not available. To circumvent this shortcoming we employ the mean-field theory in one dimension and employ magnetic Reynolds numbers in the range of $\mathrm{Re_M} = 2$ to $\mathrm{Re_M} = 10^5$. The mean quantities are spatial averages in x- and y-direction. Any change of variables only occurs in the z-direction, which can be physically interpreted as the vertical distance from the galactic mid-plane or the vertical distance from the equator of the Sun. The domain is limited to the range $0 < z < H$. Because we expect the magnetic field to develop either a symmetric or antisymmetric mode (Krause and Rädler, 1980) the boundaries at $z = 0$ are chosen accordingly such that the field is symmetric or antisymmetric about the mid-plane depending on the type of flux. In physical terms, the x- and y-components can be regarded as poloidal and toroidal components of the fields.

The driving, or energy input, comes from an imposed kinetic α effect, which has a linearly increasing profile switching sign across the equator (Fig. 3.7,

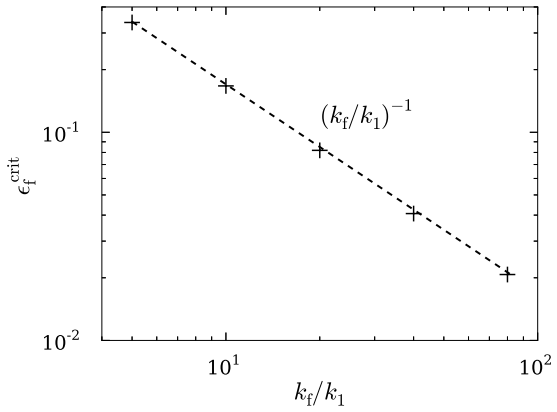

Figure 3.5: Minimal values for the normalized kinetic helicity for which large-scale dynamo action occurs in dependence of the scale separation value.

upper panel):

$$\alpha_K = \alpha_0 z/L, \tag{3.16}$$

with the size of the domain L. The total α effect is the sum of the kinetic and magnetic α effects. The latter is proportional to the current helicity and can be well approximated by the magnetic helicity, since the developing field is expected to be helical:

$$\alpha_M = \frac{\tau}{3}\overline{\boldsymbol{j}\cdot\boldsymbol{b}}/\overline{\rho} \approx \frac{\tau}{3}k_f^2\overline{\boldsymbol{a}\cdot\boldsymbol{b}}/\overline{\rho}, \tag{3.17}$$

with the turbulence correlation time τ, the small-scale current density $\boldsymbol{j}$, magnetic field $\boldsymbol{b}$ and magnetic vector potential $\boldsymbol{a}$ and the average fluid density $\overline{\rho}$.

The evolution equations for the magnetic helicity in the small and large scales are

$$\frac{\partial \overline{h}_m}{\partial t} = 2\overline{\mathcal{E}}\cdot\overline{\boldsymbol{B}} - 2\eta\overline{\boldsymbol{J}}\cdot\overline{\boldsymbol{B}} - \boldsymbol{\nabla}\cdot\overline{\boldsymbol{F}}_m, \tag{3.18}$$

$$\frac{\partial \overline{h}_f}{\partial t} = -2\overline{\mathcal{E}}\cdot\overline{\boldsymbol{B}} - 2\eta\overline{\boldsymbol{j}\cdot\boldsymbol{b}} - \boldsymbol{\nabla}\cdot\overline{\boldsymbol{F}}_f, \tag{3.19}$$

with the magnetic helicity fluxes for the small and large scales $\overline{\boldsymbol{F}}_f$ and $\overline{\boldsymbol{F}}_m$ given as

$$\overline{\boldsymbol{F}}_m = \overline{\boldsymbol{E}}\times\overline{\boldsymbol{A}}, \qquad \overline{\boldsymbol{F}}_f = \overline{\boldsymbol{e}\times\boldsymbol{a}}, \tag{3.20}$$

where $\boldsymbol{E}$ is the electric field. A term of the form $\overline{\mathcal{E}}\cdot\overline{\boldsymbol{B}}$ in equations (3.18) and (3.19) does not occur in the equation for the total magnetic helicity, because this term is only a property of the mean-fields. It makes sure that magnetic helicity is exchanged between the two scales. Equations (3.17) and (3.19)

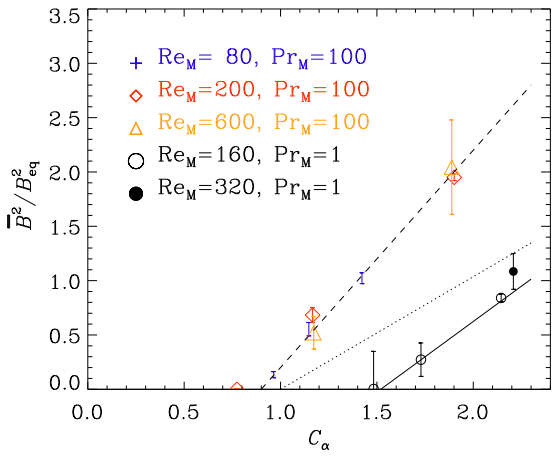

Figure 3.6: Normalized magnetic energy in the steady state in dependence of C_α for various magnetic Reynolds numbers and magnetic Prandtl numbers together with fits (dashed and solid line) and the theoretical prediction from equation (3.7) (dotted line).

give rise to the evolution equation of $\alpha_{\rm M}$, the dynamical quenching formula (Kleeorin and Ruzmaikin, 1982), expressed as

$$\frac{\partial \alpha_{\rm M}}{\partial t} = -2\eta_{\rm t} k_{\rm f}^2 \left(\frac{\overline{\boldsymbol{\mathcal{E}}} \cdot \overline{\boldsymbol{B}}}{B_{\rm eq}^2} + \frac{\alpha_{\rm M}}{\mathrm{Re_M}} \right) - \frac{\partial}{\partial z} \overline{F}_\alpha, \tag{3.21}$$

where $\overline{F}_\alpha$ is the z-component of the flux for $\alpha_{\rm M}$ given as

$$\overline{F}_\alpha = \frac{\mu_0 \overline{\rho} \eta_{\rm t} k_{\rm f}^2}{B_{\rm eq}^2} \overline{\boldsymbol{F}}_{\rm f}^z. \tag{3.22}$$

Apart from equation (3.21) we also solve the induction equation for the mean magnetic field

$$\partial_t \overline{\boldsymbol{B}} = \eta \boldsymbol{\nabla}^2 \overline{\boldsymbol{B}} + \boldsymbol{\nabla} \times (\overline{\boldsymbol{U}} \times \overline{\boldsymbol{B}} + \overline{\boldsymbol{\mathcal{E}}}) \tag{3.23}$$

and the EMF

$$\overline{\boldsymbol{\mathcal{E}}} = \alpha \overline{\boldsymbol{B}} - \eta_{\rm t} \overline{\boldsymbol{J}}. \tag{3.24}$$

It should be pointed out that no momentum or continuity equation are solved, which is chosen for simplicity and to screen off any other non-linear effects.

The form of the fluxes in equation (3.21) is chosen to be either of advective or diffusive nature. For the advective fluxes we impose a mean velocity field, which increases linearly with z (Fig. 3.7, lower panel) of the form $\overline{\boldsymbol{U}}_z = U_0 z/H$, with the scale height H, which is taken from the model used by Shukurov et al. (2006). The motivation comes from observations of galactic outflows

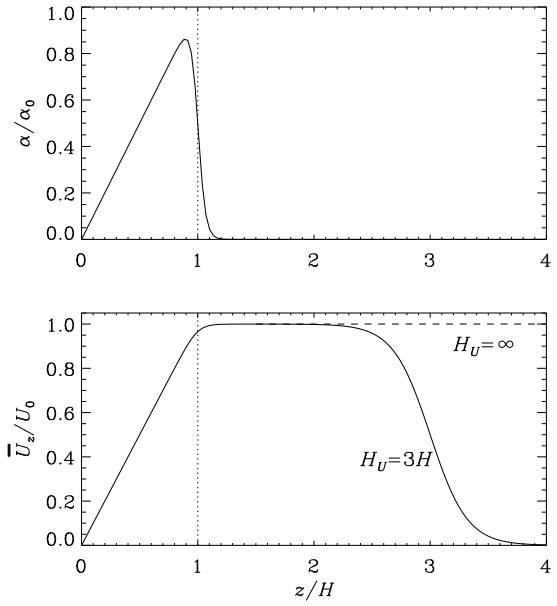

Figure 3.7: Profile of the kinetic α effect (upper panel) and the velocity profile for the case of fluxes through wind (lower panel).

where the outflow speed increases approximately linearly with distance from the galactic center (Shapiro and Field, 1976; Bregman, 1980). The wind drags the magnetic field along with magnetic helicity, which is being shed at the open boundaries. The form of open boundaries condition is $\overline{A}_{x,z} = \overline{A}_{y,z} = \overline{A}_z = 0$. This is frequently called vertical field condition, which becomes clear when writing it in terms of the magnetic field:

$$\overline{\boldsymbol{B}} = \boldsymbol{\nabla} \times \overline{\boldsymbol{A}} = \begin{pmatrix} -\overline{A}_{y,z} \\ \overline{A}_{x,z} \\ 0 \end{pmatrix}. \tag{3.25}$$

For the diffusive fluxes there is no need for open boundaries, which is why they are taken to be closed (perfect conductor), i.e. $\overline{A}_x = \overline{A}_y = 0$. Any fluxes are supposed to occur through the equator and are of the form

$$\overline{F}_\alpha = -\kappa_\alpha \frac{\partial \alpha_{\rm M}}{\partial z}, \tag{3.26}$$

with a diffusion coefficient κ_α. Since the outer boundaries are closed, the only place where diffusive fluxes can occur is at the equator.

The given setup is one of the most simple ones for which dynamo action can be expected. Under the given conditions a mean magnetic field should

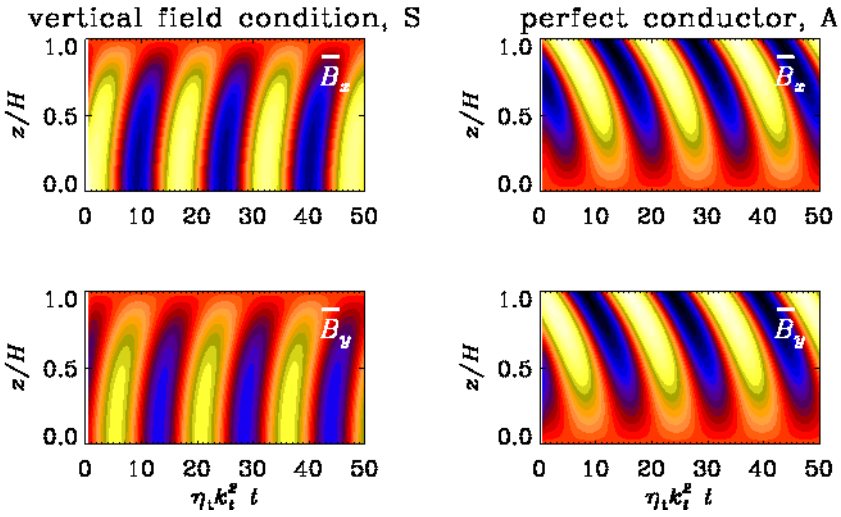

Figure 3.8: x- and y-component of the mean magnetic field for the case of an imposed wind (left panels) and no wind but diffusive fluxes through the equator (right panel) in dependence of time and the distance from the equator.

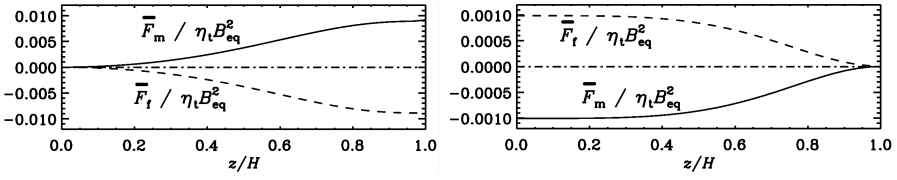

Figure 3.9: Magnetic helicity fluxes of the small- (dashed line) and large-scale fields (solid line) in dependence of the distance from the equator for the case of open boundaries and advective fluxes (left panel) and closed boundaries and diffusive fluxes (right panel).

develop after a time which is well below the resistive time. Indeed, a strong large-scale magnetic field develops and in both cases it shows an oscillatory behavior (Fig. 3.8).

Since the dynamo is working, it is now of interest to know what the effect of the fluxes is, in particular with respect to the dynamical α quenching. The advective fluxes efficiently transport small-scale magnetic helicity out of the domain (Fig. 3.9, left panel). The rate of field transport is chosen low enough not to transport too much magnetic energy out of the dynamo region, which would destroy any amplification effect. It is strong enough to alleviate the catastrophic α quenching and allow the dynamo to work even at high magnetic Reynolds numbers (Fig. 3.10, left panel). Diffusive fluxes through the equator (Fig. 3.9, right panel) allow to alleviate the catastrophic α quenching as well

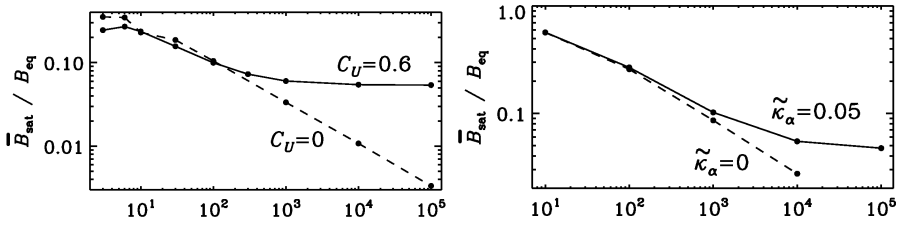

Figure 3.10: Mean magnetic field strength at saturation in dependence of the magnetic Reynolds number $\mathrm{Re_M}$ for the case with wind (left panel, solid line) and with diffusive fluxes (right panel, solid line). The cases without any fluxes are represented by dashed lines. Advective an diffusive fluxes efficiently alleviate the catastrophic quenching. Without fluxes catastrophic quenching makes the saturation field drop like $\mathrm{Re_M}^{-1/2}$.

(Fig. 3.10, right panel). For physical systems like the Sun this implies that as long as it shuffles around magnetic helicity between both hemispheres, such that the small-scale magnetic helicity diminishes, catastrophic α quenching can be alleviated.

Contrary to the algebraic quenching formalisms, where a heuristic formula is proposed for the decrease of α as the mean-field saturates, the dynamical quenching formalism provides a more self-consistent approach. The alleviation of the quenching comes not unexpectedly. As long as the advective wind does not remove too much magnetic energy it merely sheds the magnetic helicity and the α effect does not get quenched. This case is of physical relevance for the galactic dynamo for which small-scale magnetic helicity can be shed through the observed galactic winds. The diffusive fluxes are relevant for systems like our Sun where there exists a sign reversal for the kinetic helicity across the equator. As consequence also the magnetic helicity switches signs (Blackman and Brandenburg, 2003). Fluxes out of the Sun can be mediated by coronal mass ejections, which occur at regions where the magnetic field is helical. For example, Warnecke et al. (2011) found that in a spherical shell dynamo, the flux through the surface from ejections is almost twice as large as the flux through the equator.

4. Gauge Dependencies

Take advantage of the ambiguity in the world.
Look at something and think what else it might be.

Roger von Oech

4.1 Magnetic Helicity Fluxes

The gauge dependence of magnetic helicity fluxes makes the findings in section 3.2 worth revisiting. Since the alleviation of catastrophic α quenching is a physical effect it should not depend on the gauge. By choosing different gauges we investigate which the physically relevant quantities for the large-scale dynamo are. Further, we now consider direct numerical simulations where we can actually measure the diffusive helicity fluxes, which previously were merely imposed, and determine their strength compared to resistive terms and in dependence of the magnetic Reynolds number. The aim of **Paper III** is to first reproduce such diffusive fluxes through the equator (mid-plane) of the domain in direct numerical simulations. By varying the gauge it is observed how that flux changes and how it can retain its physical significance.

Uncurling the induction equation for the magnetic field leaves the freedom to choose a scalar field Ψ, which leaves the physics untouched. The induction equation has then the form

$$\frac{\partial \boldsymbol{A}}{\partial t} = \boldsymbol{U} \times \boldsymbol{B} - \eta \boldsymbol{J} - \boldsymbol{\nabla}\Psi. \tag{4.1}$$

Choosing the form of Ψ fixes the gauge. In the time evolution equation Ψ appears only in the flux term like

$$\boldsymbol{F} = \boldsymbol{E} \times \boldsymbol{A} + \Psi \boldsymbol{B}. \tag{4.2}$$

Here we consider three different gauges. For the Weyl gauge $\Psi = 0$. In the resistive gauge the gauge field Ψ is expressed in terms of the magnetic vector potential as $\Psi = \eta \boldsymbol{\nabla} \cdot \boldsymbol{A}$, which adds a diffusion component to equation (4.1). The pseudo-Lorentz gauge is equivalent to the Lorentz gauge, except that the speed of light c is replaced by the isothermal speed of sound $c_{\rm s}$:

$$\frac{\partial \Psi}{\partial t} = -c_s^2 \boldsymbol{\nabla} \cdot \boldsymbol{A}. \tag{4.3}$$

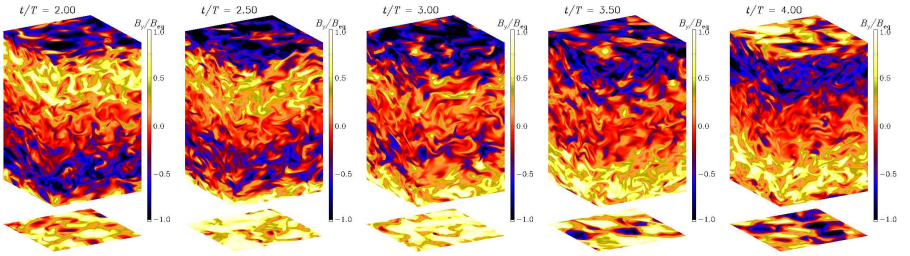

Figure 4.1: Snapshots of the y component of the magnetic field at the domain's periphery for different times. The field reversal occurs at about two resistive times. The time unit is $\tau_{\rm res} = (u_{\rm rms} k_{\rm m}^2/(3k_{\rm f}))^{-1}$.

The equations, which we solve are the same as for the periodic α^2 dynamo in section 3.1, given by equations (3.9)–(3.11), except that the induction equation is enhanced by the gradient of the gauge field Ψ. Similar to the setup used in section 3.2 we impose a forcing function $\boldsymbol{f}$ in the momentum equation, which drives the dynamo. Here, $\boldsymbol{f}$ is again a helical function, which gives rise to turbulent helical motions. The equator, or mid-plane, of the system is defined by the profile of the amplitude of $\boldsymbol{f}$, which is linearly increasing in z and zero at the mid-plane ($z = 0$). This setup resembles somewhat the Sun where kinetic helicity switches sign across the equator. All the boundaries are chosen to be periodic. The domain is a cuboid with sizes $L_x = L_y = L_z/2$, such that both halves are cubes of the same size.

Our setup is motivated by previous work by Mitra et al. (2010) in wedge-shaped domains with helical forcing, which switched sign across the equator. The resulting large-scale magnetic field showed oscillations and equatorward migration. This kind of dynamo produces oscillating magnetic fields of opposite sign in both hemispheres (Fig. 4.1), which is what is seen in Fig. 3.8 in the prefect conductor case.

Unlike in the one-dimensional case, there is no other constraint at the equator, but the vanishing of $\boldsymbol{f}$. The previously imposed diffusive small-scale magnetic helicity fluxes should arise naturally in the three dimensional case. To measure them we need to decompose the field into a small-scale and large-scale part, as it is used in mean-field theory (§ 2.2.1). By fully expanding the terms occurring in the evolution equation for the magnetic helicity for the small and large scales

$$\partial_t \overline{h}_{\rm m} = 2\overline{\boldsymbol{\mathcal{E}}}\cdot\overline{\boldsymbol{B}} - 2\eta\overline{\boldsymbol{J}}\cdot\overline{\boldsymbol{B}} - \boldsymbol{\nabla}\cdot\overline{\boldsymbol{F}}^{\rm H}_{\rm m}, \tag{4.4}$$

$$\partial_t \overline{h}_{\rm f} = -2\overline{\boldsymbol{\mathcal{E}}}\cdot\overline{\boldsymbol{B}} - 2\eta\overline{\boldsymbol{j}\cdot\boldsymbol{b}} - \boldsymbol{\nabla}\cdot\overline{\boldsymbol{F}}^{\rm H}_{\rm f}, \tag{4.5}$$

we can monitor each term of equation (4.5). We are interested in the Fickian

diffusion term of the form

$$\overline{\boldsymbol{F}}_{\rm f}^{\rm H} = -\kappa_{\rm f}\boldsymbol{\nabla}\overline{h}_{\rm f}, \tag{4.6}$$

with the diffusion coefficient $\kappa_{\rm f}$. It should be noted that for the fluxes in equation (4.5) not only Fickian diffusion is possible, though the other options need a large-scale velocity field (advective fluxes) or large-scale shear (Vishniac and Cho, 2001). The gradient of the magnetic helicity density $\boldsymbol{\nabla}\overline{h}_{\rm f/m}$, can be measured from the simulations.

Measuring the small-scale magnetic helicity fluxes $\overline{\boldsymbol{F}}_{\rm f}^{\rm H}$ through the equator for the three different gauges at a specific time reveals some significant deviation from each other (Fig. 4.2, upper panel). Instead of fluxes at a given time instance, the physically relevant quantity is the flux at the statistically steady state. For that we need to average over fluctuations which is denote as $\langle . \rangle_t$. Doing so leads to

$$\langle \partial_t \overline{h}_{\rm f} \rangle_t = 0, \tag{4.7}$$

$$\langle \boldsymbol{\nabla} \cdot \overline{\boldsymbol{F}}_{\rm f}^{\rm H} \rangle_t = -2\langle \overline{\boldsymbol{\mathcal{E}}} \cdot \overline{\boldsymbol{B}} \rangle_t - 2\langle \eta \overline{\boldsymbol{J}} \cdot \overline{\boldsymbol{B}} \rangle_t. \tag{4.8}$$

Since the RHS of equation (4.8) is gauge-invariant the LHS has to be so as well. Hence $\overline{\boldsymbol{F}}_{\rm f}^{\rm H}$ is gauge-invariant for the statistically steady state. This is reproduced in the lower panel of figure 4.2.

Comparing the terms of the helicity evolution equation of the small-scale field in equation (4.5) (Fig. 4.3, upper panel) reveals that away from the boundaries the time-averaged terms $2\overline{\boldsymbol{\mathcal{E}}} \cdot \overline{\boldsymbol{B}}$ and $2\eta\,\overline{\boldsymbol{j} \cdot \boldsymbol{b}}$ balance very well. This implies that the fluxes are small and the major part of the magnetic helicity vanishes resistively. This is true for the magnetic Reynolds number $\mathrm{Re_M} = 68$. The reminder of the change in helicity comes through the fluxes (Fig. 4.3, middle panel). The fluxes themselves can be well approximated via Fickian diffusion fluxes, see figure 4.3 lower panel, where we compare the inferred Fickian diffusion with the actual fluxes.

In the present investigation magnetic Reynolds numbers between 2 and 68 are used. In that range the fluxes do not show any clear tendency and can be considered to be independent of $\mathrm{Re_M}$, while the terms $2\overline{\boldsymbol{\mathcal{E}}} \cdot \overline{\boldsymbol{B}}$ and $2\eta\,\overline{\boldsymbol{j} \cdot \boldsymbol{b}}$ scale with $\mathrm{Re_M}$. For the fluxes to play any significant role during the dynamo process they need to be comparable to the term $2\overline{\boldsymbol{\mathcal{E}}} \cdot \overline{\boldsymbol{B}}$. Before that no significant alleviation of catastrophic α quenching can be observed (Fig. 4.4, upper panel). For higher magnetic Reynolds numbers it is expected that diffusive fluxes increase such that they become determining and α quenching gets alleviated. This happens for $\mathrm{Re_M}$ at which $\kappa_{\rm f}\nabla^2\overline{\boldsymbol{a} \cdot \boldsymbol{b}} \approx 2\eta\,\overline{\boldsymbol{j} \cdot \boldsymbol{b}}$. The magnetic Reynolds number for which the terms become comparable is $\mathrm{Re_M} \approx 4600$ (see **Paper III** for details). This result is based on linear extrapolations. Recent findings (Del Sordo et al., 2012) have shown that this breaks down and that the diffusive flux divergence

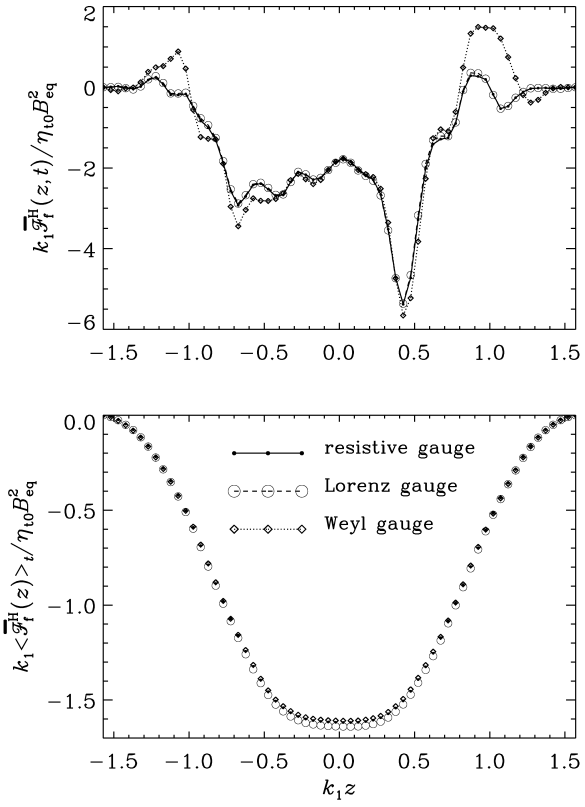

Figure 4.2: Small-scale magnetic helicity fluxes at a random time (upper panel) and their time average (lower panel) for the three gauges. The time averaged quantities are clearly gauge independent.

becomes approximately independent of $\mathrm{Re_M}$ for $\mathrm{Re_M} \approx 100$ and above. For even higher $\mathrm{Re_M}$ the diffusive flux divergence approaches $2\overline{\boldsymbol{\mathcal{E}}} \cdot \overline{\boldsymbol{B}}$.

The gauge dependence of magnetic helicity fluxes is not physically relevant in the statistically steady state, where fluxes are balanced by physical quantities which do not depend on the gauge. Fickian diffusion gives a good proxy for the total magnetic helicity flux. That shows that no other fluxes occur in this particular setup. For low magnetic Reynolds numbers the segregation of magnetic helicity in small- and large-scale parts, expressed in the $2\overline{\boldsymbol{\mathcal{E}}} \cdot \overline{\boldsymbol{B}}$ term, is not balanced by the fluxes. For high, and physically relevant $\mathrm{Re_M}$, we could estimate that it will balance at $\mathrm{Re_M} \approx 4600$. Simulations with such high $\mathrm{Re_M}$ have yet to be realized, but will shed more light on this topic (see Del Sordo et al. (2012)).

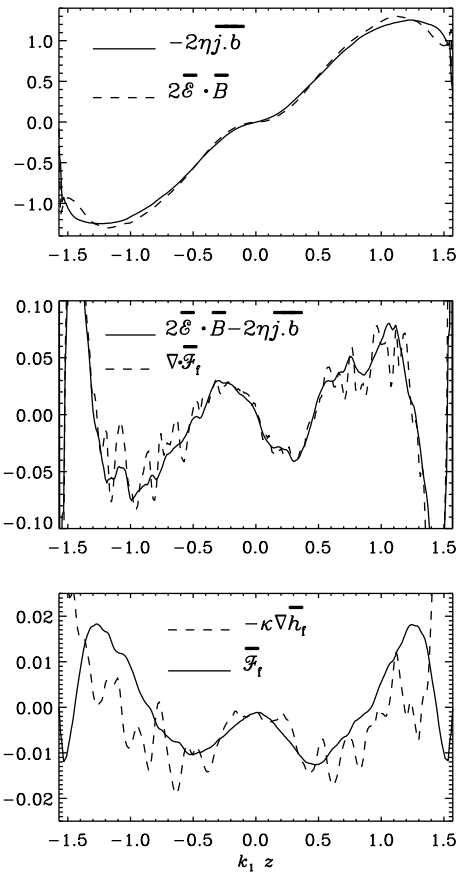

Figure 4.3: z profile of the terms of equation (4.5) (upper two panels) and a comparison between the actual magnetic helicity fluxes and the Fickian diffusion term from equation (4.6).

4.2 The Advecto-Resistive Gauge

In **Paper IV** properties of the magnetic helicity density and its fluxes are examined in a gauge belonging to the advective gauge-families. They are called advective, because velocity shows up as a term which advects the magnetic helicity (Hubbard and Brandenburg, 2011). This should be contrasted to e.g. the resistive gauge, where no such term arises. Gauge-dependent magnetic helicity fluxes mean gauge dependent magnetic helicity transport. The way this physically important quantity is transported in a turbulent environment is part of the present discussion and contrasted with the transport of a passive scalar. Numerical analysis for the advective gauge proves to lead to numerical instabilities, which do not arise in other gauges. To still investigate this gauge a

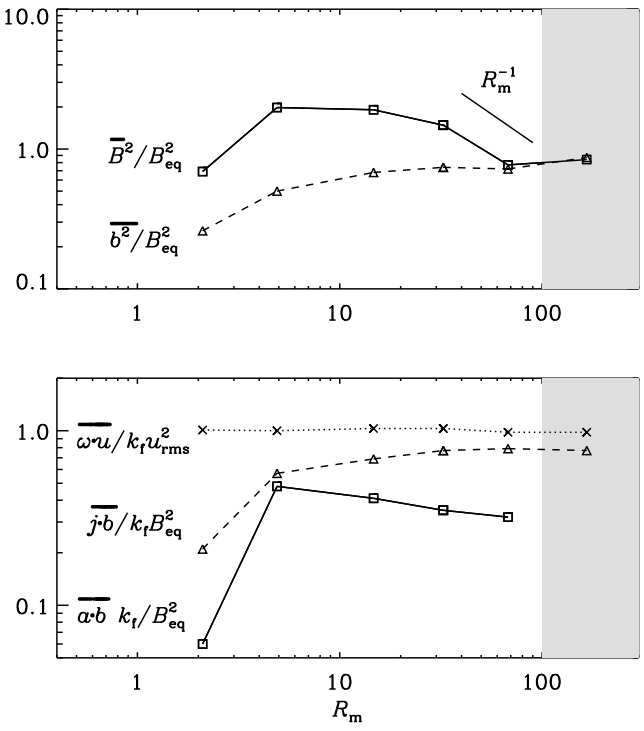

Figure 4.4: Dependence of the normalized magnetic energy in the small and large scale with the magnetic Reynolds number (upper panel). Kinetic, current and magnetic helicity, each appropriately normalized, in dependence of $\mathrm{Re_M}$ (lower panel).

universal approach is used for stabilizing the numerical experiment. For that the numerically stable resistive gauge is used for the evolution, while simultaneously solving an evolution equation for the gauge field, which provides the transformation.

In order to distinguish quantities in different gauges a superscript is used, e.g. $\boldsymbol{A}^{\mathrm{r}}$ for the resistive gauge. The induction equation for the magnetic vector potential in the popular resistive gauge reads

$$\frac{\partial \boldsymbol{A}^{\mathrm{r}}}{\partial t} = \boldsymbol{U} \times \boldsymbol{B} + \eta \boldsymbol{\nabla}^2 \boldsymbol{A}^{\mathrm{r}}, \tag{4.9}$$

where the magnetic resistivity η is here assumed to be constant in space. This gauge is numerically stable and commonly used for simulations. Its stability arises form the diffusion term, which reduces any artificial small-scale fluctuations or discontinuities.

In the advective gauge the induction equation reads

$$\frac{\mathrm{D}A_i^{\mathrm{a}}}{\mathrm{D}t} = -U_{j,i}A_j^{\mathrm{a}} - \eta J_i. \tag{4.10}$$

Its form is similar to the gauge, which will be mainly discussed here, which is the advecto-resistive gauge with induction equation

$$\frac{\mathrm{D}A_i^{\mathrm{ar}}}{\mathrm{D}t} = -U_{j,i}A_j^{\mathrm{ar}} + \eta\boldsymbol{\nabla}^2 A_i^{\mathrm{ar}}. \tag{4.11}$$

Any transformation between two gauge-dependent fields can be achieved by adding a gauge field. The transformation between the resistive and advecto-resistive gauge reads

$$\boldsymbol{A}^{\mathrm{ar}} = \boldsymbol{A}^{\mathrm{r}} + \boldsymbol{\nabla}\Lambda^{\mathrm{r:ar}}, \tag{4.12}$$

with the gauge field $\Lambda^{\mathrm{r:ar}}$. The superscript r:ar signifies the original and target gauge. Looking at the induction equation (4.11) it becomes clear why this is called advecto-resistive. It incorporates the advective nature of the advective gauge, as well as the resistive term from the resistive gauge.

Solving the equations in the advecto-resistive gauge leads to numerical instabilities. Therefore we have to make use of the stable resistive gauge and apply the gauge transformation Eq. (4.12) for computing any gauge-dependent quantities in the advecto-resistive gauge. The field $\Lambda^{\mathrm{r:ar}}$ will then have to obey its own evolution equation (see appendix B in **Paper IV** for the derivation):

$$\frac{\mathrm{D}\Lambda^{\mathrm{r:ar}}}{\mathrm{D}t} = -\boldsymbol{U}\cdot\boldsymbol{A}^{\mathrm{r}} + \eta\boldsymbol{\nabla}^2\Lambda^{\mathrm{r:ar}}. \tag{4.13}$$

Applying equation (4.11) together with equation (4.13) is referred to as the Λ method. Although the advecto-resistive gauge is numerically unstable, we will use it in some simulations and discuss where the instability comes from.

Magnetic helicity transport is crucial in dynamo theory (see **Paper I**, **Paper II**, **Paper III** and references therein). In both, the resistive and advecto-resistive gauge, the time evolution of the magnetic helicity density is determined by a resistive term and fluxes given as

$$\frac{\partial h^{\mathrm{a}}}{\partial t} = -2\eta\boldsymbol{J}\cdot\boldsymbol{B} - \boldsymbol{\nabla}\cdot\boldsymbol{F}^{\mathrm{a}}, \tag{4.14}$$

$$\frac{\partial h^{\mathrm{r}}}{\partial t} = -2\eta\boldsymbol{J}\cdot\boldsymbol{B} - \boldsymbol{\nabla}\cdot\boldsymbol{F}^{\mathrm{r}}, \tag{4.15}$$

$$\frac{\partial h^{\mathrm{ar}}}{\partial t} = -2\eta\boldsymbol{J}\cdot\boldsymbol{B} - \boldsymbol{\nabla}\cdot\boldsymbol{F}^{\mathrm{ar}}, \tag{4.16}$$

with the magnetic helicity fluxes $\boldsymbol{F}^{\mathrm{a}}$, $\boldsymbol{F}^{\mathrm{r}}$ and $\boldsymbol{F}^{\mathrm{ar}}$ given by

$$\boldsymbol{F}^{\mathrm{a}} = h^{\mathrm{a}}\boldsymbol{U} + \eta\boldsymbol{J}\times\boldsymbol{A}^{\mathrm{a}}, \tag{4.17}$$

$$\boldsymbol{F}^{\mathrm{r}} = h^{\mathrm{r}}\boldsymbol{U} - (\boldsymbol{U}\cdot\boldsymbol{A}^{\mathrm{r}} + \eta\boldsymbol{\nabla}\cdot\boldsymbol{A}^{\mathrm{r}})\boldsymbol{B} + \eta\boldsymbol{J}\times\boldsymbol{A}^{\mathrm{r}}, \tag{4.18}$$

$$\boldsymbol{F}^{\mathrm{ar}} = h^{\mathrm{ar}}\boldsymbol{U} - \eta(\boldsymbol{\nabla}\cdot\boldsymbol{A}^{\mathrm{ar}})\boldsymbol{B} + \eta\boldsymbol{J}\times\boldsymbol{A}^{\mathrm{ar}}. \tag{4.19}$$

Fluxes of magnetic helicity in all cases appear as advective fluxes ($h\boldsymbol{U}$) and resistive fluxes ($\eta\boldsymbol{J}\times\boldsymbol{A}$). In the limit of ideal MHD and incompressible fluids, i.e. $\eta = 0$ and $\boldsymbol{\nabla}\cdot\boldsymbol{U} = 0$, equation (4.14) is formally the same as the evolution of a passive scalar:

$$\frac{\mathrm{D}h^{\mathrm{a}}}{\mathrm{D}t} = 0. \tag{4.20}$$

The resistive gauge breaks this analogy, caused by fluxes in the direction of the magnetic field of the form $\boldsymbol{U}\cdot\boldsymbol{A}^{\mathrm{r}}\boldsymbol{B}$, called turbulently diffusive fluxes. The varying nature of the fluxes is one issue addressed in **Paper IV**.

The solved equations are the momentum equation (2.2) with the helical forcing term $\boldsymbol{f}$, the continuity equation (2.3) and the induction equation whose form depends on the method and gauge. The isotropic forcing $\boldsymbol{f}$ provides the energy input and ensures a dynamo is working. For the induction equation we either choose the purely resistive gauge with equation (4.9), the pure advecto-resistive gauge with equation (4.11) or the resistive gauge combined with the evolution equation for the gauge field Λ (Eq. (4.13)), which is used to compute magnetic helicity and its fluxes via the transformation

$$h^{\mathrm{ar}} = h^{\mathrm{r}} + \boldsymbol{\nabla}\Lambda\cdot\boldsymbol{B}. \tag{4.21}$$

Additionally the evolution of a passive scalar C

$$\frac{\mathrm{D}C}{\mathrm{D}t} = \kappa\nabla^2 C, \tag{4.22}$$

is solved to compare its dynamics with the magnetic helicity, where κ is the diffusivity of the passive scalar. The triply periodic boundary conditions imposed lead to a slow saturation of the mean magnetic field.

The helical forcing $\boldsymbol{f}$ injects kinetic energy, which gets transformed into magnetic energy via the α effect. Together with the magnetic field also the magnetic helicity increases (Fig. 4.5). Choosing to directly solve the induction equations in the advecto-resistive gauge causes the simulation to develop high gradients of $\boldsymbol{A}$, which should not affect $\boldsymbol{B}$, but numerically they do. The values grow to such high values that the simulation stops. Changing the simulation's resolution does not have any significant effect on the stability. It is an intrinsic property of the gauge choice.

The instability arises from numerically taking the derivative of $\boldsymbol{A}^{\mathrm{ar}}$ in equation (4.11). The expansion of the Laplacian operator shows that there is a hidden curl operator applied on the gradient of the gauge field $\Lambda^{\mathrm{r:ar}}$ of the form

$$\boldsymbol{\nabla}^2\boldsymbol{A}^{\mathrm{ar}} = \boldsymbol{\nabla}(\boldsymbol{\nabla}\cdot\boldsymbol{A}^{\mathrm{ar}}) - \boldsymbol{\nabla}\times(\boldsymbol{\nabla}\times\boldsymbol{A}^{\mathrm{r}} + \boldsymbol{\nabla}\times(\boldsymbol{\nabla}\Lambda^{\mathrm{r:ar}}))\,. \tag{4.23}$$

The curl of the gradient should of course vanish. Numerically, however, it does not, which leads to an artificial increase of magnetic field in the small scales.

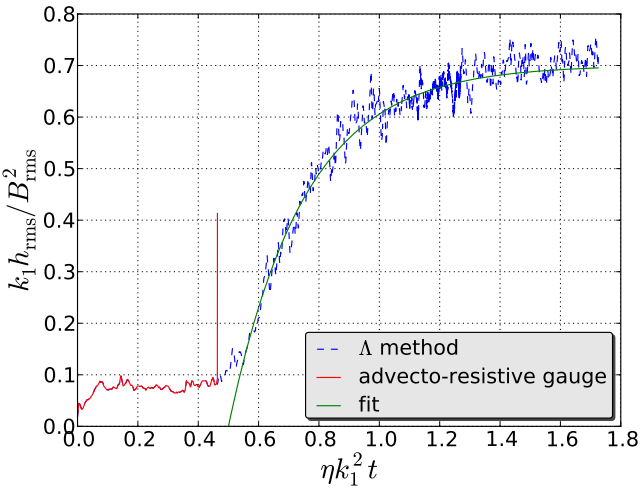

Figure 4.5: Normalized root mean square value of the magnetic helicity for the direct advecto-resistive gauge (solid red line) and the Λ method (dashed line) together with a fit (solid green line).

As consequence also the velocity increases due to the Lorentz force and the simulation crashes. Using the Λ method, this issue is circumvented.

The total magnetic helicity in this setup with periodic boundaries is gauge-invariant. Its density distribution, however, is not. Any difference between the resistive and advecto-resistive gauges on density distribution, in the absence of compressibility effects, can only be caused by the fluxes, which is reflected in the root mean square of the magnetic helicity $h_{\rm rms}$. For the resistive gauge, in contrast to the advecto-resistive gauge, additional flux terms appear in the form of $(\boldsymbol{U}\cdot\boldsymbol{A}^{\rm r})\boldsymbol{B}$, which can diminish the transport. Consequently, magnetic helicity will be transported less efficiently into scales of the turbulent eddies for the resistive, than for the advecto-resistive gauge. This effect increases as the fluid Reynolds number increases. Highly varying concentrations mean an increase of the root mean square value $h_{\rm rms}$. Indeed, we can reproduce this feature for the advecto-resistive gauge (Fig. 4.6, left panel) and provide an approximate law for its quantitative behavior given by

$$\frac{k_1 h^{\rm ar}}{B_{\rm rms}^2} = c{\rm Re}_{\rm M}^{-a}(1+b{\rm Re}_{\rm M}^{2a}), \tag{4.24}$$

with the fit parameters a and b. This effect is absent for the resistive gauge (Fig. 4.6, right panel).

We compare the dynamics of the passive scalar with the magnetic helicity density by evaluating their spectra (Fig. 4.7). In the kinematic regime, where resistive terms are negligible, the magnetic helicity spectrum shows a drop at

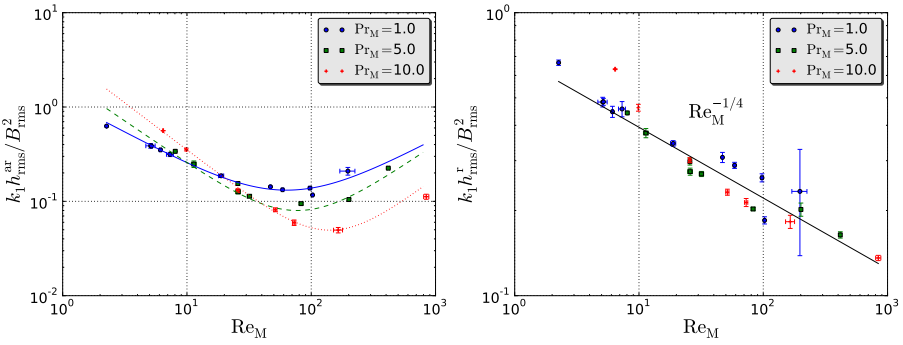

Figure 4.6: Time averaged values of the normalized magnetic helicity for the kinematic phase in dependence of the magnetic Reynolds number for different Prandtl numbers. The advecto-resistive case (left panel) clearly shows a different behavior (model by equation (4.24)) from the resistive case (right panel), which shows a power law dependence.

high wave numbers, which is different from the advecto-resistive gauge. This drop comes from the more effective way of dissipating high spatial variations of $\boldsymbol{A}$, due to the resistive term in the induction equation. This term is of course also present in the advecto-resistive gauge, but due to the efficient transport of helicity into smaller scales, thanks to the advective term, high k components get constantly supplied from low k. This comparison holds true even for the non-linear regime. There it can be seen that $h^{\rm r}$ develops a peak at the forcing scale $k_{\rm f}$, which is to be expected from dynamo theory where the magnetic field peaks there. Of similar reasons is the peak of the passive scalar. The turbulent helical fluid motions trap it into this scale. Since there is no way of transporting C other than advection it retains its peak at the forcing scale $k_{\rm f}$. Because for the advecto-resistive case there is helicity transport into smaller scales the peak vanishes and we see a flatter profile.

In summary we present an effective way to circumvent numerical instabilities arising form the gauge choice, by solving for an evolution equation for the gauge field Λ. In this context one may ask why not solve directly for the physical quantities and applying an inverse curl operator when computing helicities. One reason is the divergence freeness of the magnetic field ($\boldsymbol{\nabla}\cdot\boldsymbol{B}=0$), which is automatically assured when solving for the magnetic vector potential $\boldsymbol{A}$. It makes it also easier to compute the magnetic helicity for which no inverse curling is needed. The differing fluxes result in some interesting consequences for the helicity transport. In the advecto-resistive gauge the co-moving local magnetic helicity density remains closer to its initial value, except at small scales where it leads to a high k tail (Fig. 4.7). The resistive gauge makes the helicity evolve akin a passive scalar. It should be remembered that the only

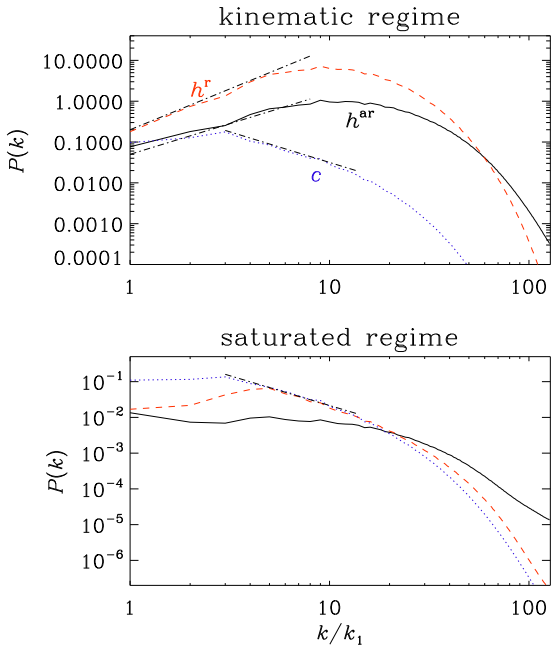

Figure 4.7: Power spectra for the magnetic helicities h^{r}, h^{ar} and the passive scalar C for $k_{\mathrm{f}}/k_1 = 5$. The additional transport term causes h^{ar} to have a flatter profile and higher values at high k, in contrast to h^{r}.

distinction in time evolution between $\boldsymbol{A}^{\mathrm{r}}$ and $\boldsymbol{A}^{\mathrm{ar}}$ comes from the gauge transformation Eq. (4.13). So the difference in the transport comes solely from the gauge field Λ.

5. Topology

The characters emerge from my rather twisted mind.
That's another enjoyable part of the job making stuff up.

Jonathan Kellerman

Two field configurations are topologically different if they cannot be transformed one into another with a homeomorphic transformation. In other words, without the aid of magnetic reconnection they cannot be converted into each other. This does not mean that reconnection necessarily changes the topology of the field. Even with reconnection the topology can be conserved. Topology is to be contrasted with geometry, which describes the shape of the field.

Field line topology particularly affects relaxation processes (Berger and Field, 1984; Ricca, 2008). Since the field cannot be shaped in any arbitrary way, relaxation does not occur totally freely. This aspect, with connection to magnetic helicity, is discussed in **Paper V**. Magnetic helicity is, however, not the only quantifier for field line topology (Yeates and Hornig, 2012). There exists an infinite number of topological invariants. Whether those can play any role in field line relaxation is discussed in **Paper VI**.

5.1 Flux Linking and Magnetic Helicity

The most common way of quantifying the topology of magnetic fields is the magnetic helicity (Moffatt, 1969), which gives a measure for the mutual linkage of magnetic fields lines. Two mutually liked magnetic flux rings, which do not possess any internal twisting nor are self-interlinked, are an instructive example for the analogy between linkage and magnetic helicity (see Fig. 1.3). It could be shown by Moffatt (1969) that the number of mutual linkage n is related to the total magnetic helicity H_M as

$$H_\mathrm{M} = \int_V \boldsymbol{A} \cdot \boldsymbol{B} \, \mathrm{d}V = 2n\phi_1\phi_2, \tag{5.1}$$

where ϕ_i are the magnetic fluxes through the field lines

$$\phi_i = \int_{S_i} \boldsymbol{B} \cdot \mathrm{d}\boldsymbol{S}. \tag{5.2}$$

Conservation of magnetic helicity for low magnetic resistivity, as it is the case for astrophysical applications, makes it an ideal invariant, even when magnetic reconnection occurs (Taylor, 1974).

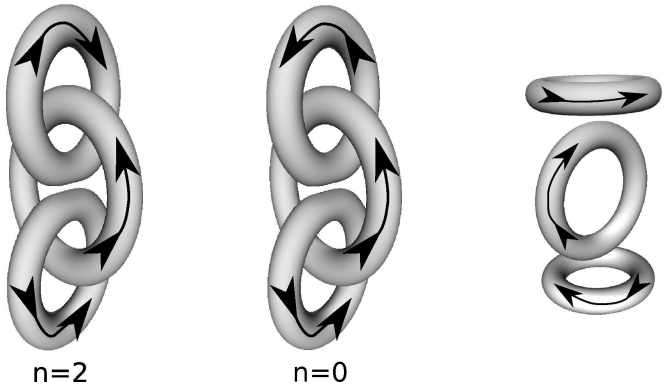

Figure 5.1: Isosurfaces of the magnetic energy for the helical linked (left panel), non-helical linked (central panel) and unlinked (right panel) magnetic field configuration. The direction of the magnetic field is pictured by the arrows.

With this colorful picture of the magnetic helicity it is obvious that with its presence any relaxation must be impeded, as long as the system is not breaking up field lines. This characteristics is captured in the realizability condition Eq. (2.49), which imposes a lower limit on the magnetic energy in presence of magnetic helicity. Of course one can make up non-helical configurations with linked flux tubes. If their topology was conserved that property would need to be captured in a higher order invariant (Ruzmaikin and Akhmetiev, 1994; Komendarczyk, 2010). The question then is what is more important: the actual topology (linking) or the magnetic helicity. This is addressed in **Paper V**.

As a showcase, three field configurations are investigated (Fig. 5.1). Two of them consist of three interlinked magnetic flux rings of finite width and no internal twisting. The reversal of the direction of the field in one of the two outer rings changes the magnetic helicity content from an appreciable value to zero. As reference configuration to compare with, we use the same three rings without any linkage (Fig. 5.1, right panel).

The three magnetic field configurations are used as initial conditions. The cross section and magnetic flux in the tubes is the same for all three rings. The radii of the outer rings are R_0 and for the inner ring is $R = 1.2R_0$. As profile for the magnetic field strength a Gaussian is used, which has the advantage of being a smooth function. The relaxation characteristics is investigated within the framework of resistive MHD. For that we solve the usual MHD equations (2.1)–(2.3) without any forcing $\boldsymbol{f}$. The initial values of velocity and density are $\boldsymbol{U}_0 = 0$ and $\rho_0 = 1$. The initial magnetic flux through the tubes is $\Phi = 0.1 c_{\rm s} R_0^2 \sqrt{\mu_0 \rho_0}$, which is small enough to ignore compression effects and consider the density as constant. Magnetic resistivity η is set to a value as small as is numerically admissible for the sake of magnetic helicity conserva-

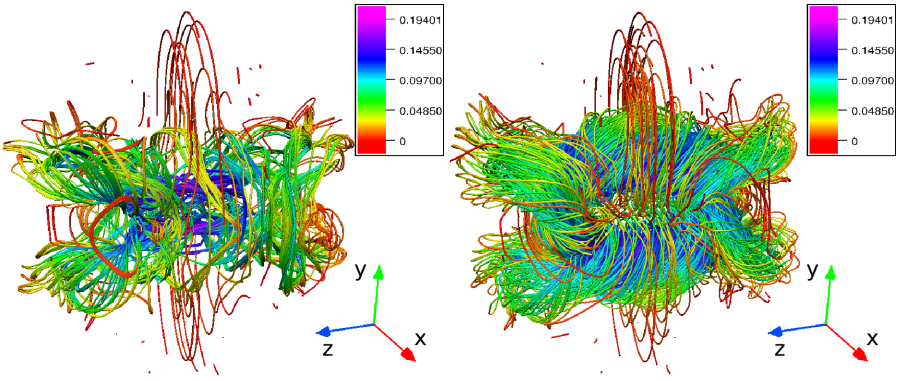

Figure 5.2: Magnetic stream lines after 4 Alfvénic times for the interlocked triple-ring configurations. The non-helical case (left) loses most of its initial structure, while the helical case (right) retains it and distinct tubes can still be observed.

tion. To make sure magnetic helicity cannot escape, the domain boundaries are assumed periodic. Time is measured in Alfvénic times, which in the present cases is only a fraction of the resistive time:

$$T_{\mathrm{A}} = \sqrt{\mu_0 \rho_0} R_0^3 / \Phi. \tag{5.3}$$

As times evolves each outer ring shrinks due to magnetic tension and diffusion. When the field lines touch local reconnection events occur which change the shape of the field. For the non-helical interlocked field the initial structure vanishes after only a few Alfvénic times (Fig. 5.2, left panel), while for the helical configuration the initial topology remains conserved (Fig. 5.2, right panel).

During the relaxation magnetic energy gets lost into heat[1] through reconnection events and resistive effects. The rate of loss depends on how fast the system can attain its equilibrium energy. For the non-helical case it can be seen that energy is dissipated quickly (Fig. 5.3) – in fact as quickly as for the non-interlocked test configuration. The mere linking does apparently not hinder the field to decay almost freely. For the helical case the realizability condition imposes severe restrictions on the relaxation. In practice this means a slow loss of magnetic energy on a resistive time scale on which also the magnetic helicity decays.

In summary we can confirm the importance of the realizability condition for relaxation processes. The naïve interpretation of linked flux tubes whose

[1]No energy equation is solved here. So the dissipated energy cannot be reused by any means, like buoyancy.

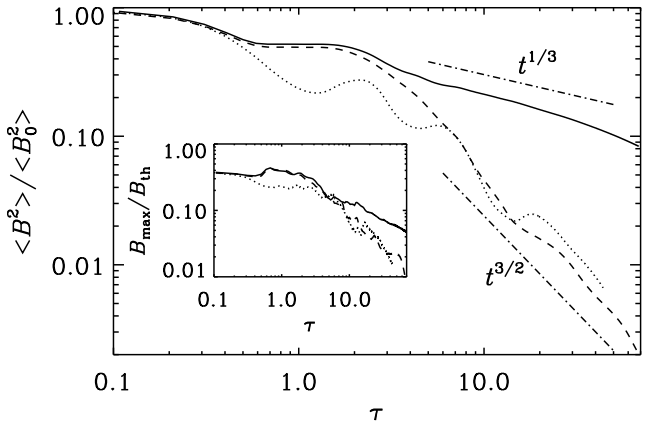

Figure 5.3: Magnetic energy evolution for the three rings configurations normalized by their initial value. The helical interlocked configuration retains its energy content more successfully (solid line), while the linked non-helical one (dashed lines) and the non-linked case (dotted line) lose energy quickly at approximately the same rate.

dynamics is restricted by the linkage does not hold. The only essential quantity is the magnetic helicity.

5.2 Beyond Magnetic Helicity

Since there exists an infinite number of topological invariants it should be investigated if magnetic helicity is always the sole determinant in magnetic field dynamics. To address this question we perform in **Paper VI** similar relaxation experiments as in **Paper V** with field configurations in the shape of knots and links. The investigated magnetic field configurations are the n-foil knots, the Borromean rings and the IUCAA knot (Fig. 5.4). Similar numerical experiments have been carried out for ideal MHD (Maggioni and Ricca, 2009) where no reconnection events could take place.

The family of n-foil knots, of which the trefoil knot is the simplest example, has only helical members. By increasing their complexity with parameter n, their magnetic energy increases, as well as the magnetic helicity. The Borromean rings and IUCAA knot are both non-helical configurations. Yet, they are topologically non-trivial and cannot be undone without braking the field lines. For the Borromean rings there exists a higher order topological invariant, which is conserved in ideal MHD, but gets destroyed during magnetic reconnection (Ruzmaikin and Akhmetiev, 1994).

As in the case of the triple ring configurations of **Paper V** the bound-

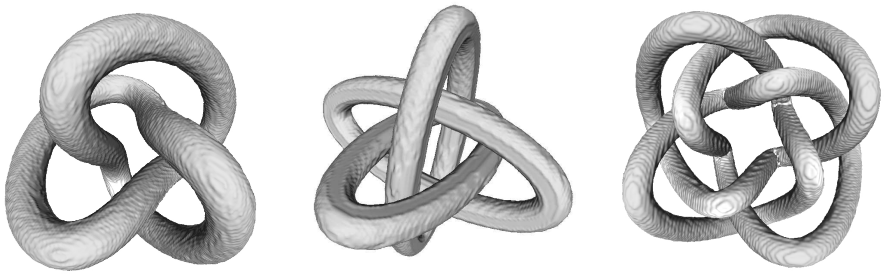

Figure 5.4: Isosurfaces of the magnetic energy for the initial field configurations trefoil knot (left panel), Borromean rings (middle panel) and the IUCAA knot (right panel).

aries are chosen to be periodic in order to conserve magnetic helicity. For the same reason the magnetic resistivity η is chosen as small as computationally possible. The governing equations for this problem are the same as for the triple rings case, which are equations (2.1)–(2.3) without forcing $\boldsymbol{f}$. We use the magnetic field configurations shown in Fig. 5.4 as initial conditions and let the systems relax.

The relaxation of the n-foil knots does not give any surprises. The magnetic helicity imposes restrictions on the field relaxation, which gets more pronounced as the complexity of the configuration is increased. The power laws of $t^{-1/3}$ found in **Paper V** for the energy decay of the helical triple ring configuration could only be found for the most complex member of this family studied here, the 7-foil knot. The least complex, the trefoil knot, shows a $t^{-2/3}$ behavior. This characteristics comes from the increasing ratio of magnetic helicity to magnetic energy as the complexity grows with n. The energy increases linearly with complexity, while the magnetic helicity grows quadratically. Consequently, the realizability condition slows down the energy decay more effectively (see **Paper VI** for details).

The Borromean rings show an intriguing property, which distinguishes this configuration form other non-helical configurations. As the field evolves and tries to relax it undergoes reconnection events. Those events transform the linked rings into two separate rings, which are twisted (Fig. 5.5). The twist is of opposite sign, due to magnetic helicity conservation. The energy decay is not of the form $t^{-3/2}$, but of t^{-1} (Fig. 5.6). This we attribute to the occurrence of separate helical structures, which evolve independently. Similar reconnection steps for this configuration were shown in a theoretical work by Ruzmaikin and Akhmetiev (1994) where it was proposed that the Borromean rings should reconnect into a trefoil knot and three figure eight knots with opposite helicity. After further reconnection the system should end up with two un-knots and six

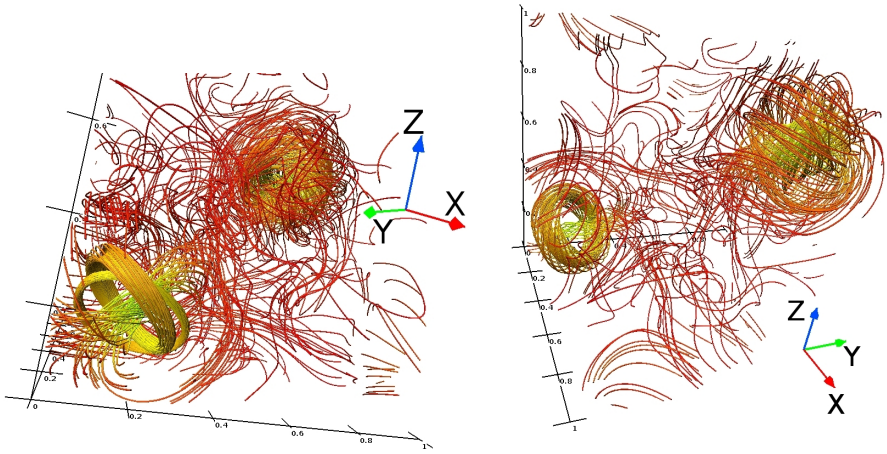

Figure 5.5: Magnetic stream lines for the Borromean field configuration after 70 Alfvénic times (left) and 78 (right). The initial configuration is totally lost and replaced by two twisted fields.

figure eight knots of which three have opposite sign of the other three, in order to conserve helicity. Making the interpretation that those figure eight knots are the internal twist of the final un-knots we can conclude that their findings match with our simulation results. The presence of magnetic helicity in the separate twisted tubes imposes restrictions on the relaxation expressed in the realizability condition Eq. (2.49).

The IUCAA knot also shows a relaxation behavior, which lies in between the decay speed of the helical and non-helical triple-ring configurations (Fig. 5.6). This illustrates that even non-helical fields reveal non-trivial behavior. Since no such helical structures as for the Borromean rings appear, we are tempted to speculate about higher order invariants, which inhibit the field decay.

Once again the importance of the realizability condition is confirmed. For the n-foil knots we see that the higher the magnetic helicity content is compared to the magnetic energy the stronger is the inhibition from the realizability condition to let the field relax into a lower energy state. The surprisingly slow decay of the Borromean rings can be attributed to the emergence of helical structures, which evolve independently and where the realizability condition imposes restrictions on the relaxation. For the IUCAA knot no such explanation could be found and one may again speculate about higher order topological invariants. One way of doing this is by applying the concept of topological flux functions, which can be used to uniquely identify the topology of the magnetic field configuration (Yeates and Hornig, 2012). Defining such a flux function requires a field with a preferential direction as they occur for instance in tokamaks. This, nevertheless, does not restrict one of applying

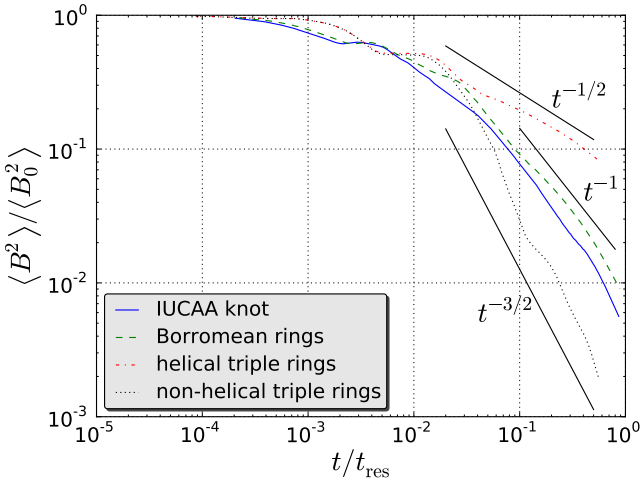

Figure 5.6: Normalized magnetic energy for the linked triple-ring configurations, the Borromean rings and the IUCAA knot together with power laws to guide the eye.

this concept on knots and links, since they can always be represented as braids in a periodic domain.

A potential physical applications of the topologies discussed here is the explanation of magnetic cavities observed in the intergalactic medium (Ruszkowski et al., 2007; Pfrommer and Jonathan Dursi, 2010) which show high resistance against Kelvin-Helmholtz instability. It has been shown by Braithwaite (2010) that tangled fields enhance the stability of bubbles during relaxation. It is yet to be demonstrated that they can reduce the Kelvin-Helmholtz instability.

6. Conclusions

Denn die Menschen glauben an die Wahrheit dessen,
was ersichtlich stark geglaubt wird.

All things are subject to interpretation.
Whichever interpretation prevails at a given time
is a function of power and not truth.

Friedrich Nietzsche

Magnetic helicity is a fundamental quantity in the dynamics of magnetic fields in the Universe. Its importance has been appreciated in several previous works ranging from the implication of its conservation in dynamos (Pouquet et al., 1976) to the constraint it imposes in field relaxation (Moffatt, 1978).

Its conservation causes the turbulent large-scale dynamo to grow on resistive time scales, which, for astrophysical objects like the Sun and galaxies, are much longer than the dynamical time scales we observe. The saturation strength of the large-scale magnetic field is fundamentally affected by magnetic helicity as well and is drastically reduced to values much lower than those observed. In **Paper I** it is discussed how the saturation characteristics change with the relevant parameters, which are the scale separation ratio between the size of the turbulent motion and the system and the relative amount of injected kinetic helicity. As predicted by mean-field estimates (Blackman and Brandenburg, 2002), the saturation magnetic energy of the large-scale field scales proportionally to the scale separation ratio and the injected relative helicity. Further, for the large-scale dynamo to operate, the critical value for the normalized helicity of the small-scale turbulent motions scales inversely proportional to the scale separation ratio. This leads to an excellent confirmation of the mean-field predictions. Previous findings (Pietarila Graham et al., 2012), which suggest different scaling behaviors, arguably lack proper analysis of the magnetic field of the large-scale dynamo.

The form of the forcing function, which drives the dynamo, is usually taken to be of helical nature, which leads to helical magnetic fields. Amongst these different behaviors for the large-scale field is that of **Paper I**, where for most parts a helical forcing random in time is used. There are three different magnetic field averages competing during the resistive saturation, the xy-, xz- and yz-averaged magnetic fields. Only one survives at the end of the saturation phase. For the ABC-flow forcing an intriguing behavior is seen, where the

three modes oscillate in time with a phase shift of $2\pi/3$. The nature of this oscillation is not understood yet and has to be investigated further.

A reduction of magnetic helicity in the small scales can be obtained via various kinds of fluxes (Rogachevskii and Kleeorin, 2000; Vishniac and Cho, 2001; Subramanian and Brandenburg, 2004, 2006) of which not all can efficiently reduce its amount such that catastrophic α quenching gets alleviated. Two kinds of fluxes are considered in **Paper II**. Advective fluxes, mediated by a wind, efficiently transport the magnetic field together with small-scale magnetic helicity out of the system. Physically speaking this can be interpreted as coronal mass ejections with helical magnetic fields or as a galactic wind. Diffusive fluxes within closed domains between parts of opposite helicity are also efficient enough to alleviate catastrophic α quenching and allow for high mean magnetic saturation field strengths for high magnetic Reynolds numbers. In practice this means that the mere reshuffling of magnetic helicity within a closed system, through e.g. the equator, reduces sufficiently the amount of "hostile" helicity of small-scale fields.

The gauge dependence of magnetic helicity does not constitute a problem for the physical effect of magnetic helicity fluxes. Choosing different gauges, namely the Weyl, resistive and pseudo Lorentz gauges does not change the time-averaged helicity fluxes through the mid-plane of the domain (**Paper III**). This is shown for equations in the steady state, where fluxes of magnetic helicity appear together with quantities which are gauge-independent, which implies that also the fluxes must be gauge-independent.

Choosing different gauges can be useful to test magnetic helicity transport. It can, however, lead to numerical instabilities arising from large gradient contributions in the magnetic vector potential when computed numerically. This pitfall can be circumvented by solving the evolution equations in a numerically stable gauge and applying a gauge transformation for computing gauge-dependent quantities like the magnetic helicity density or its fluxes (**Paper IV**). Transport and distribution of magnetic helicity in the advecto-resistive gauge is found to differ significantly from the advective gauge. It can transport magnetic helicity more efficiently to smaller length scales, especially in the case of low magnetic resistivity.

Topological constraints coming from field line linkage or knotting is contrasted against the realizability condition, which only holds as long as the configuration is helical. Of course the realizability condition can already be regarded as describing constraints coming from the field's topology. There are, however, non-helical setups, which are topologically non-trivial. For those we find in **Paper V** that their linkage has little effect on the field relaxation. This is compared with non-linked setups, which show the same energy decay characteristics. In **Paper V** the restrictions on the field's dynamics solely arises

from the magnetic helicity content, rather than the actual linkage.

The content of magnetic helicity in knotted flux tubes is shown to scale like the number of crossings obtained from an appropriate 2d projection of the configuration (**Paper VI**). The relaxation characteristics of those helical knots is, however, not directly comparable with the previous helical triple-ring configuration. The reason is simply the increasing helicity content with increasing complexity of the knots. Non-helical setups exhibit relaxation speeds, which are found to lie somewhere in between those for helical and non-helical fields. For one configuration, namely the Borromean rings, this departure is attributed to the occurrence of separated helical flux rings for which the realizability condition holds. In the case of the non-helical IUCAA knot no such explanation is possible, which is why one can speculate about higher order topological invariants. Fortunately magnetic helicity is not the only quantifier for the field's topology. There exists an infinite number of such quantities. One of them is the fixed point index, which has been shown to impose another restriction on the field's relaxation (Yeates et al., 2010).

7. Outlook

Dazu gibt er dem Menschen die Hoffnung:
sie ist in Wahrheit das übelste der Übel,
weil sie die Qual der Menschen verlängert.

Hope in reality is the worst of all evils
because it prolongs the torments of man.

Friedrich Nietzsche

Gradually we are extending our grasps on how magnetic helicity is formed and in which ways it affects astrophysical systems. The work presented here is rather abstract, yet fundamental. To make predictions for physical systems more realistic simulations have to be performed.

The helical forcing used in turbulent dynamos leads to a separation of magnetic helicity in the small and large scales. As main consequence the large-scale magnetic field grows to considerable values. In **Paper I** we also use the ABC-flow forcing, which leads to rotating averages for the mean magnetic field. The nature of this rotation and exact characteristics are not known. Further investigations on that would show if the rotation keeps on in time or if the equilibrium solution is stationary or not.

Apart form magnetic helicity, also cross helicity, the correlation of the turbulent velocity with the turbulent magnetic field, takes part in the generation of the magnetic field (Yoshizawa, 1990). Most of the work done so far (Yoshizawa and Yokoi, 1993; Yokoi, 1996, 1999) has been done analytically. Numerical simulations have yet to show the importance of cross helicity for the mean-field dynamo. A setup would consist of a rotating stratified medium where a weak mean magnetic field is imposed. That should lead to the growth of magnetic energy. The mean-field calculations would then be compared to the direct numerical simulations using the test-field method (Schrinner et al., 2005).

In the intergalactic medium X-ray cavities have been observed (Ruszkowski et al., 2007; Pfrommer and Jonathan Dursi, 2010) which are hot under-dense regions. They rise due to buoyancy and are expected to be shred into small pieces due to the Kelvin-Helmholtz instability (von Helmholtz, 1868, Thomson, 1871, Chandrasekhar, 1961). They seem, however, to survive for millions of years, which is a considerably longer time than predicted by simulations. The Kelvin-Helmholtz instability has been shown to be suppressed by helical

magnetic fields, which makes the fluid more stable against shredding. Numerical simulations of helical magnetic cavities have to be conducted in order to quantitatively understand their stability in the intergalactic medium. Such configurations could be under-dense regions in a cooler stratified medium with gravity. Inserting a helical magnetic field in those cavities should then show stabilizing effects.

Magnetic helicity is not the only topological invariant. There exists an infinite number of invariants, which can be used to characterize the topology of magnetic field lines. Just a few of them are useful for diffusive fields, which fill the whole volume. Two of them are the magnetic helicity (Moffatt, 1969) and the fixed point index (Yeates et al., 2010). The latter was shown to restrict the relaxation of the magnetic field for particularly braided magnetic fields. As a next step I will use this method for configurations which are topologically equivalent to knots and links. In this context a topological flux function is defined whose change in the fixed points gives a proxy for the magnetic reconnection rate. This will enable us to determine whether magnetic resistivity changes the reconnection rate and if magnetic helicity is conserved during reconnection.

Sammanfattning

Skillnaden mellan geniet och dumheten är
att geniet har sin begränsning.

Torvald Gahlin

Magnetfält spelar en betydande roll inom astrofysiken. De underlättar transporten av rörelsemängdsmoment och kan därför förklara varför solen roterar relativt långsamt. Magnetfälts uppkomst förklaras genom dynamoeffekten där turbulent rörelse ger upphov till magnetisk energi. Sådana magnetfält är helikala, dvs. deras fältlinjer är länkade. Att de är helikala har vidsträckta konsekvenser för deras dynamik.

Att förklara hur sådana fält kommer till stånd är en del av det här avhandlingen. Det visas att det magnetiska heliciteten hindrar det storskaliga fältet att utvecklas. Tiden som fältet behöver att formas blir längre än solens ålder och intensiteten minskas till ett löjligt litet värde. Hur magnetfältet påverkas av turbulensens egenskaper är avhandlingens första del. Det visas hur strömmen av magnetisk helicitet lindrar den dämpade effekten för magnetfältets tillväxt. Fysikaliskt betyder det att koronamassutkastningar stödjer fältets utveckling.

Den magnetiska helicitetens beroende på gaugen leder till frågan om hur den kan vara fysikaliskt relevant. I den andra delen av avhandlingen undersöker jag hur gaugen påverkar transporten av helicitet och hur dess fysikaliska relevans räddas. Det visas att i det stationära tillståndet tidsmedelvärdet av strömmen inte är gaugeberoende. Å andra sidan är spektrumet beroende på gaugen. I den advecto-resistiva gaugen, till exempel, transporteras magnetisk helicitet mer effektivt till små skalor, vilket ger upphov till en flatare profil.

Magnetisk helicitet kan tolkas som länkar av magnetfältlinjer. Därmed blir det tydligt att fältet inte kan relaxera fritt. I den tredje och sista delen undersöker jag hur länkning och heliciteten påverkar fältets dynamik. Det visas att enbart länkning inte är tillräckligt för att inskränka dynamiken; det behövs helicitet. Från ytterligare numeriska experiment visas det att andra topologiska kvantiteter också kan spela en roll i fältets relaxation. Hittills är det inte känt vilka.

References

V. I. Arnold. The asymptotical hopf invariant and its applications. *Sel. Math. Sov.*, 5, 1974. 19

G. K. Batchelor. On the Spontaneous Magnetic Field in a Conducting Liquid in Turbulent Motion. *Roy. Soc. Lond. Proc. Ser. A*, 201:405–416, 1950. 19

M. A. Berger and G. B. Field. The topological properties of magnetic helicity. *J. Fluid Mech.*, 147:133–148, 1984. 18, 49

E. G. Blackman and A. Brandenburg. Dynamic Nonlinearity in Large-Scale Dynamos with Shear. *Astrophys. J.*, 579:359–373, 2002. 5, 25, 26, 57

E. G. Blackman and A. Brandenburg. Doubly Helical Coronal Ejections from Dynamos and Their Role in Sustaining the Solar Cycle. *Astrophys. J.*, 584:L99–L102, 2003. 35

E. G. Blackman and G. B. Field. Constraints on the Magnitude of α in Dynamo Theory. *Astrophys. J.*, 534: 984–988, 2000. 17, 30

P. L. Boyland, H. Aref, and M. A. Stremler. Topological fluid mechanics of stirring. *J. Fluid Mech.*, 403: 277–304, 2000. 22

J. Braithwaite. Magnetohydrodynamic relaxation of AGN ejecta: radio bubbles in the intracluster medium. *Month. Not. Roy. Astron. Soc.*, 406:705–719, 2010. 55

A. Brandenburg. The Inverse Cascade and Nonlinear Alpha-Effect in Simulations of Isotropic Helical Hydromagnetic Turbulence. *Astrophys. J.*, 550:824–840, 2001. 15, 27

A. Brandenburg and W. Dobler. Solar and stellar dynamos - latest developments. *Astron. Nachr.*, 323: 411–416, 2002. 17

A. Brandenburg and K. Subramanian. Astrophysical magnetic fields and nonlinear dynamo theory. *Phys. Rep.*, 417:1–209, 2005. 11, 14, 15

A. Brandenburg, A. Nordlund, R. F. Stein, and U. Torkelsson. Dynamo-generated Turbulence and Large-Scale Magnetic Fields in a Keplerian Shear Flow. *Astrophys. J.*, 446:741, 1995. 5

A. Brandenburg, W. Dobler, and K. Subramanian. Magnetic helicity in stellar dynamos: new numerical experiments. *Astron. Nachr.*, 323:99–122, 2002. 26

J. N. Bregman. The galactic fountain of high-velocity clouds. *Astrophys. J.*, 236:577–591, 1980. 33

R. F. Brown. *The Lefschetz Fixed Point Theorem*. Scott Foresman, London, 1971. 22

R. C. Canfield, H. S. Hudson, and D. E. McKenzie. Sigmoidal morphology and eruptive solar activity. *Geophys. Res. Lett.*, 26:627–630, 1999. 23

S. Chandrasekhar. *Hydrodynamic and hydromagnetic stability*. Oxford Univ. Press, 1961. 61

P. Charbonneau, M. Dikpati, and P. A. Gilman. Stability of the Solar Latitudinal Differential Rotation Inferred from Helioseismic Data. *Astrophys. J.*, 526:523–537, 1999. 19

A. R. Choudhuri, M. Schussler, and M. Dikpati. The solar dynamo with meridional circulation. *Astron. Astrophys.*, 303:L29, 1995. 19

F. Del Sordo, G. Guerrero, and A. Brandenburg. Turbulent dynamo with advective magnetic helicity flux. *arXiv:1205.3502*, 2012. 39, 40

U. Frisch, A. Pouquet, J. Léorat, and A. Mazure. Possibility of an inverse cascade of magnetic helicity in magnetohydrodynamic turbulence. *J. Fluid Mech.*, 68:769–778, 1975. 15, 26

S. E. Gibson, L. Fletcher, G. Del Zanna, C. D. Pike, H. E. Mason, C. H. Mandrini, P. Démoulin, H. Gilbert, J. Burkepile, T. Holzer, D. Alexander, Y. Liu, N. Nitta, J. Qiu, B. Schmieder, and B. J. Thompson. The structure and evolution of a sigmoidal active region. *Astrophys. J.*, 574:1021, 2002. 23, 24

A. V. Gruzinov and P. H. Diamond. Self-consistent theory of mean-field electrodynamics. *Phys. Rev. Lett.*, 72:1651–1653, 1994. 29

A. Hubbard and A. Brandenburg. Magnetic Helicity Flux in the Presence of Shear. *Astrophys. J.*, 727:11, 2011. 41

T. S. Ivanova and A. A. Ruzmaikin. A nonlinear magnetohydrodynamic model of the solar dynamo. *Sov. Astron.*, 21:479–485, 1977. 13

H. Ji. Turbulent Dynamos and Magnetic Helicity. *Phys. Rev. Lett.*, 83:3198–3201, 1999. 26

P. J. Käpylä and A. Brandenburg. Turbulent Dynamos with Shear and Fractional Helicity. *Astrophys. J.*, 699:1059–1066, 2009. 5

N. Kleeorin and I. Rogachevskii. Magnetic helicity tensor for an anisotropic turbulence. *Phys. Rev. E*, 59: 6724–6729, 1999. 30

N. Kleeorin, D. Moss, I. Rogachevskii, and D. Sokoloff. Helicity balance and steady-state strength of the dynamo generated galactic magnetic field. *Astron. Astrophys.*, 361:L5–L8, 2000. 17

N. I. Kleeorin and A. A. Ruzmaikin. Dynamics of the average turbulent helicity in a magnetic field. *Magnetohydrodynamics*, 18:116, 1982. 32

R. Komendarczyk. The third order helicity of magnetic fields via link maps. *J. Math. Phys.*, 51:122702, 2010. 50

F. Krause and K. H. Rädler. Dynamo theory of the suns general magnetic fields on the basis of a mean-field magnetohydrodynamics. In R. Howard, editor, *Solar Magnetic Fields*, volume 43 of *IAU Symposium*, page 770, 1971. 11

F. Krause and K.-H. Rädler. *Mean-field magnetohydrodynamics and dynamo theory*. Oxford, Pergamon Press, 1980. 11, 13, 25, 30

J. Léorat, U. Frisch, and A. Pouquet. Helical magnetohydrodynamic turbulence and the nonlinear dynamo problem. *Ann. N.Y. Acad. Sci.*, 257:173–176, 1975. 15

F. Maggioni and R. L. Ricca. On the groundstate energy of tight knots. *Roy. Soc. Lond. Proc. Ser. A*, 465: 2761–2783, 2009. 52

T. R. Metcalf, L. Jiao, A. N. McClymont, R. C. Canfield, and H. Uitenbroek. Is the solar chromospheric magnetic field force-free? *Astrophys. J.*, 439:474–481, 1995. 23

D. Mitra, R. Tavakol, P. J. Käpylä, and A. Brandenburg. Oscillatory Migrating Magnetic Fields in Helical Turbulence in Spherical Domains. *Astrophys. J.*, 719:L1–L4, 2010. 38

H. K. Moffatt. The degree of knottedness of tangled vortex lines. *J. Fluid Mech.*, 35:117–129, 1969. 20, 49, 62

H. K. Moffatt. *Magnetic field generation in electrically conducting fluids*. Camb. Univ. Press, 1978. 13, 15, 19, 25, 57

H. K. Moffatt and R. L. Ricca. Helicity and the Calugareanu Invariant. *Roy. Soc. Lond. Proc. Ser. A*, 439: 411–429, 1992. 20

C. Pfrommer and L. Jonathan Dursi. Detecting the orientation of magnetic fields in galaxy clusters. *Nature Physics*, 6:520–526, 2010. 55, 61

J. Pietarila Graham, E. G. Blackman, P. D. Mininni, and A. Pouquet. Not much helicity is needed to drive large-scale dynamos. *Physical Review E*, 85:066406, 2012. 5, 26, 27, 28, 29, 57

A. Pouquet, U. Frisch, and J. Léorat. Strong MHD helical turbulence and the nonlinear dynamo effect. *J. Fluid Mech.*, 77:321–354, 1976. 14, 57

E. R. Priest and T. G. Forbes. *Magnetic reconnection: MHD theory and applications*. 2000. 19, 20

R. L. Ricca. Topology bounds energy of knots and links. *Roy. Soc. Lond. Proc. Ser. A*, 464:293–300, 2008. 49

P. H. Roberts and A. M. Soward. A unified approach to mean field electrodynamics. *Astron. Nachr.*, 296: 49–64, 1975. 13

I. Rogachevskii and N. Kleeorin. Electromotive force for an anisotropic turbulence: Intermediate nonlinearity. *Phys. Rev. E*, 61:5202–5210, 2000. 58

M. Ruszkowski, T. A. Enßlin, M. Brüggen, S. Heinz, and C. Pfrommer. Impact of tangled magnetic fields on fossil radio bubbles. *Month. Not. Roy. Astron. Soc.*, 378:662–672, 2007. 55, 61

A. Ruzmaikin and P. Akhmetiev. Topological invariants of magnetic fields, and the effect of reconnections. *Phys. Plasmas*, 1:331–336, 1994. 21, 50, 52, 53

M. Schrinner, K.-H. Rädler, D. Schmitt, M. Rheinhardt, and U. Christensen. Mean-field view on rotating magnetoconvection and a geodynamo model. *Astron. Nachr.*, 326:245–249, 2005. 61

N. Seehafer. Nature of the α effect in magnetohydrodynamics. *Phys. Rev. E*, 53:1283–1286, 1996. 26

P. R. Shapiro and G. B. Field. Consequences of a New Hot Component of the Interstellar Medium. *Astrophys. J.*, 205:762–765, 1976. 33

A. Shukurov, D. Sokoloff, K. Subramanian, and A. Brandenburg. Galactic dynamo and helicity losses through fountain flow. *Astron. Astrophys.*, 448:L33–L36, 2006. 32

M. Steenbeck, F. Krause, and K.-H. Rädler. Berechnung der mittleren Lorentz-Feldstärke $\overline{\mathbf{v} \times \mathbf{B}}$ für ein elektrisch leitendes Medium in turbulenter, durch Coriolis–Kräfte beeinflusster Bewegung. 21a:369–376, 1966. 11, 12

K. Subramanian and A. Brandenburg. Nonlinear Current Helicity Fluxes in Turbulent Dynamos and Alpha Quenching. *Phys. Rev. Lett.*, 93:205001, 2004. 30, 58

K. Subramanian and A. Brandenburg. Magnetic Helicity Density and Its Flux in Weakly Inhomogeneous Turbulence. *Astrophys. J.*, 648:L71–L74, 2006. 58

J. B. Taylor. Relaxation of toroidal plasma and generation of reverse magnetic fields. *Phys. Rev. Lett.*, 33: 1139–1141, 1974. 19, 49

A. G. Tevzadze, L. Kisslinger, A. Brandenburg, and T. Kahniashvili. Magnetic fields from qcd phase transitions. *Astrophys. J.*, 759:54, 2012. 20

W. Thomson. Hydrokinetic solutions and observations. *Philos. Mag.*, 42:362–377, 1871. 61

S. I. Vaĭnshteĭn and F. Cattaneo. Nonlinear restrictions on dynamo action. *ApJ*, 393:165–171, 1992. 14

S. I. Vaĭnshteĭn and Y. B. Zel'dovich. Origin of Magnetic Fields in Astrophysics (Turbulent "Dynamo" Mechanisms). *Sov. Phys. Usp.*, 15:159–172, 1972. 19

E. T. Vishniac and J. Cho. Magnetic Helicity Conservation and Astrophysical Dynamos. *Astrophys. J.*, 550: 752–760, 2001. 30, 39, 58

H. von Helmholtz. Über discontinuierliche Flüssigkeits-Bewegungen. *Monatsberichte der Königlichen Preussische Akademie der Wissenschaften zu Berlin*, 23:215–228, 1868. 61

J. Warnecke, A. Brandenburg, and D. Mitra. Dynamo-driven plasmoid ejections above a spherical surface. *Astron. Astrophys.*, 534:A11, 2011. 35

L. Woltjer. On hydromagnetic equilibrium. *Proceedings of the National Academy of Science*, 44:833–841, 1958. 19

A. R. Yeates and G. Hornig. Unique Topological Characterization of Braided Magnetic Fields. *arXiv:1208.2286*, 2012. 49, 54

A. R. Yeates, D. H. Mackay, and A. A. van Ballegooijen. Evolution and distribution of current helicity in full-sun simulations. *Astrophys. J.*, 680:L165, 2008. 23

A. R. Yeates, G. Hornig, and A. L. Wilmot-Smith. Topological constraints on magnetic relaxation. *Phys. Rev. Lett.*, 105:085002, 2010. 21, 23, 59, 62

N. Yokoi. Large-scale magnetic fields in spiral galaxies viewed from the cross-helicity dynamo. *Astron. Astrophys.*, 311:731–745, 1996. 61

N. Yokoi. Magnetic-field generation and turbulence suppression due to cross-helicity effects. *Physics of Fluids*, 11:2307–2316, 1999. 61

A. Yoshizawa. Self-consistent turbulent dynamo modeling of reversed field pinches and planetary magnetic fields. *Phys. Fluids B*, 2:1589–1600, 1990. 61

A. Yoshizawa and N. Yokoi. Turbulent magnetohydrodynamic dynamo for accretion disks using the cross-helicity effect. *Astrophys. J.*, 407:540–548, 1993. 61